Edited by Yahachi Saito

Carbon Nanotube and Related Field Emitters

Fundamentals and Applications

WILEY-VCH Verlag GmbH & Co. KGaA

The Editor

Prof. Yahachi Saito
Nagoya University
Dept. of Quantum Engineering
Furo-cho, Chikusa-ku
Nagoya 464-8603
Japan

Library of Congress Card No.: applied for

British Library Cataloguing-in-Publication Data
A catalogue record for this book is available from the British Library.

Bibliographic information published by the Deutsche Nationalbibliothek
The Deutsche Nationalbibliothek lists this publication in the Deutsche Nationalbibliografie; detailed bibliographic data are available on the Internet at <http://dnb.d-nb.de>.

Cover Design Formgeber, Eppelheim
Typesetting Laserwords Private Limited, Chennai, India
Printing and Binding Strauss GmbH, Mörlenbach

Printed in the Federal Republic of Germany
Printed on acid-free paper

ISBN: 978-3-527-32734-8

8
Field Emission Microscopy of Multiwall CNTs

Yahachi Saito

8.1
Introduction

Field emission microscopy (FEM) enables imaging of the spatial distribution of the emitted electron current from an electron emitter by using a phosphor screen as anode. The emitter is usually mounted on a heating wire for cleaning the emitter surface. The electron emission is strongly affected by surface structures, local states, and the presence of adsorbates, and is reflected in the FEM patterns. Thus, FEM provides important information on the emission mechanism and surface phenomena on a carbon nanotube (CNT) [1, 2].

CNTs are one of the ideal materials as field emitters because they possess (i) needlelike shape with a sharp tip, (ii) high chemical stability, (iii) high mechanical strength, (iv) low carbon atom mobility, and (v) high electrical and thermal conductivity. The needlelike morphology with an extremely small radius of curvature at the tip is the most prominent advantage of CNTs as an electron emitter. When an electric field is applied to a conductor with a sharp tip, the field concentrates at the sharp point. The field strength at the tip surface is inversely proportional to the radius of curvature r of the tip [3]. The surface of CNTs is inert and stable against residual gas molecules in a vacuum vessel because of the chemical stability of graphite material which constitutes CNTs. The high mechanical strength (tensile strength $\sim$100 GPa [4]) of CNT emitters enables them to endure the high stress caused by electrostatic forces (Maxwell tension). Together with this robustness, the low mobility of carbon atoms in CNTs helps them retain their original shape even under a high electric field. Finally, since CNTs, especially multiwall carbon nanotubes (MWNTs) formed by arc discharge, have high electrical and thermal conductivity, CNTs can transport and emit electrons at high current density (about 10^7 A cm^{-2}) through their tubular walls [5].

This chapter focuses on FEM studies carried out mainly on MWNTs so far. In addition to fundamental properties of CNT field emitters, the molecular images and dynamics of adsorbates on CNT electron emitters revealed by FEM are presented. FEM on single-wall carbon nanotubes (SWNTs) is dealt with in Chapter 10.

Carbon Nanotube and Related Field Emitters: Fundamentals and Applications. Edited by Yahachi Saito

ISBN: 978-3-527-32734-8

8.2
FEM of Carbon Nanotubes

8.2.1
FEM Measurement

For FEM studies, employment of a single, isolated CNT fixed to the apex of a metal needle may be ideal. A few techniques to fabricate such pointed emitters are described in Chapter 2. However, the single CNT emitters prepared under a scanning electron microscope (SEM) [6] are usually covered with contaminants (hydrocarbon deposit) during the SEM observation. Electrophoresis is an alternative method to attach a thin bundle of CNTs to the tip of a metal needle [7], though the control of the number of CNTs in an attached bundle is difficult. The simple and easy method is to glue a bulk bundle of as-grown CNTs to the tip of a heating loop (e.g., a tungsten filament with diameter of 0.15 mm) by using a conductive paste [8]. The last method keeps the tips of the CNTs clean, but an enormous number of CNTs protrude out at the end of the bundle.

A schematic of an FEM apparatus is shown in Figure 8.1. The emitter tip of the CNTs is placed at about 30 mm distance from a phosphor screen, on which field emission (FE) patterns are observed. The base pressure of the FEM vacuum chamber is typically 10^{-7}–10^{-8} Pa. A negative voltage of 0.6–1.6 kV is applied to the emitter relative to the screen.

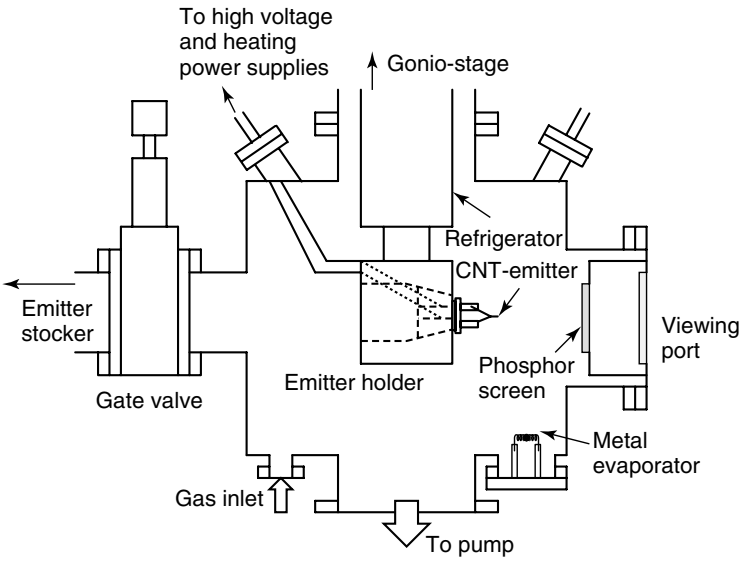

Figure 8.1 Schematic of an FEM apparatus.

8.2.2
MWNTs with Clean Surfaces

MWNTs produced by the arc-discharge technique (Chapter 1) are highly graphitized (i.e., composed of well-developed graphene layers) and thus have high structural perfection. The ends of arc-grown MWNTs are capped by graphite layers with polyhedral shapes (Chapter 1). In order to give a positive curvature to a hexagonal sheet, pentagons (five-membered carbon ring) have to be introduced to the sheet; six pentagons are required to have a curvature of 2π steradians (i.e., a hemispherical cap). The portion where a pentagon is located extrudes like the vertex of a polyhedron, while the other flat regions are made of hexagons.

Typical FEM images of MWNT emitters with clean surfaces are shown in Figure 8.2. Clean CNT tips are obtained by heating at about 1000 °C for a few minutes in an ultrahigh vacuum chamber (e.g., 10^{-8} Pa) during which the

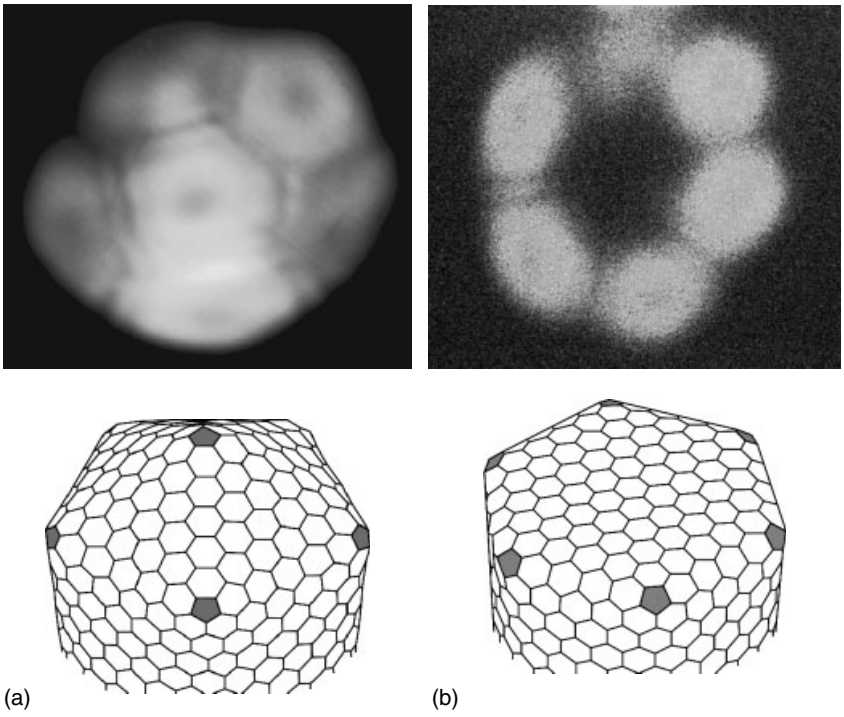

Figure 8.2 Upper panel: typical FEM images of MWNT emitters with clean surfaces. Six pentagonal rings are arranged in fivefold (a) and sixfold symmetry (b). Lower panel: structural models of CNT tips giving the FEM patterns in the upper panel.

adsorbates on CNT surfaces desorb [9]. Six pentagonal rings arranged in fivefold (Figure 8.2a) and sixfold symmetry (Figure 8.2b) can be observed. Each pentagonal region contains a small dark spot at its center. It should also be noted that interference fringes are observed between the neighboring pentagons. Structural models of CNT tips that would give the FEM patterns are shown in the lower panel in Figure 8.2.

Since the pentagons are locally extruding like vertices, the electric field around them would be stronger than that on other flat regions. In addition, it is theoretically indicated that the pentagon site has a higher density of states (DOS) of electrons near the Fermi level E_F than the normal hexagon site [10]. Therefore, the electron tunneling through the pentagons are expected to occur dominantly.

Such patterns (called *pentagon patterns* hereafter) change when gas molecules adsorb on the CNT cap. An adsorbed molecule is usually imaged as a bright spot in the FEM picture, giving rise to an abrupt increase in the emission current [9]. Similar stepwise fluctuations of emission current are also frequently observed in FE sources made of other materials [11, 12]. The origin of the stepwise changes is the adsorption and desorption of molecules on the surface of the emitter. Though most adsorbed molecules in the FEM images appear as simple, bright spots (structureless), some molecules exhibit characteristic shapes reflecting the molecular structure as described in the next section.

Emission patterns from open-ended MWNTs, which were prepared by the oxidation processes, showed bright ''doughnutlike'' annular rings, reflecting the geometry of the CNT tip [13].

8.2.3
FEM Patterns Depending on Tip Radius

FEM of MWNTs with closed caps shows clear pentagon images, but that of SWNTs, as described in Chapter 10, does not show pentagonal rings but dim (blurred) patterns which resemble scanning tunneling microscope (STM) images of C_{60} fullerenes. Experimental study using CNTs with different apex radii [14] suggested that the difference in the FEM images originates from the difference in the radius of curvature of CNT tips; the ''pentagon'' patterns are observed for CNTs with apex radii larger than about 2 nm, whereas the ''dim'' patterns correspond to smaller apex radii.

According to the argument on the spatial resolution of FEM [15, 16], resolutions of 0.2 and 0.35 nm are possible for emitters with tip radius of 1 and 4 nm, respectively. However, it is not enough to resolve individual atoms on the CNT caps. Since the pentagon–pentagon separation s_{p-p} on a CNT cap is roughly the same as the radius of curvature of the tip [14], the s_{p-p} which differentiates the patterns is presumed to be approximately 2 nm.

8.3
Field Emission from Adsorbates on an MWNT

8.3.1
Molecules

8.3.1.1 Hydrogen

Figure 8.3 shows a time-sequential series of FEM patterns from an MWNT exposed to hydrogen gas at a pressure of 1.3×10^{-6} Pa and the corresponding changes in the emission current [17]. The pentagon pattern characteristic of a clean MWNT cap just after flashing (Figure 8.3a) changed to FEM patterns in which one or two small bright spots appeared on the pentagon pattern as shown in Figure 8.3b and c, and a slight increase in the emission current occurred concurrently with the appearance of a bright spot. The number and the position of bright spots changed randomly, indicating frequent adsorption and desorption of hydrogen molecules on the CNT cap preferentially on pentagon sites where the electric field is locally the strongest. After the FE measurement for 11 min with an emission current of 50–100 nA, the hydrogen gas was evacuated and the CNT emitter was subjected to flashing. By this cleaning process, the emission pattern recovered to the original clean pattern, suggesting that hydrogen molecules are inert for the surfaces of MWNTs under this FE condition.

8.3.1.2 Nitrogen

Figure 8.4 shows two types of FEM image of an adsorbate in an atmosphere of nitrogen gas of 8×10^{-7} Pa [18]. A bright spot that appears on a pentagon site changes its brightness and shape. The image is ''cocoon'' shaped (Figure 8.4a and b)

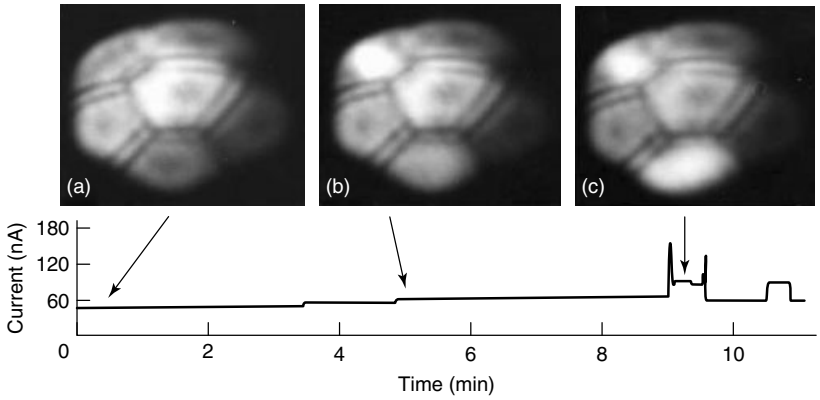

Figure 8.3 Time-sequential series of FEM patterns from an MWNT exposed to hydrogen gas at pressure of 1×10^{-8} Torr and the corresponding changes in the emission current. (Reprinted with permission from K. Hata, A. Takakura, and Y. Saito, *Ultramicroscopy* **95** (2003) 107. Copyright 2003, Elsevier.)

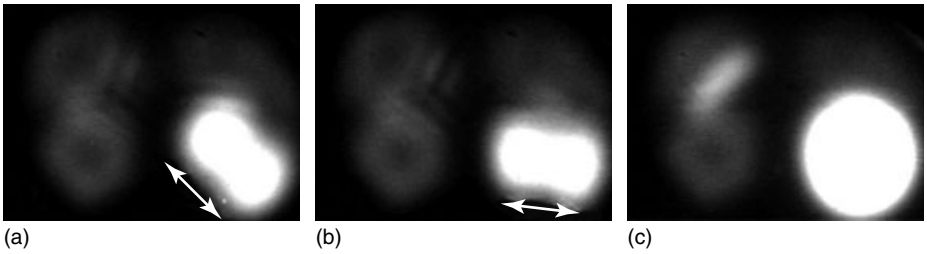

Figure 8.4 Two types of FEM pattern of a nitrogen molecule. (a) and (b) ''cocoon''-shaped images with different orientations, and (c) bright circular spot. (Reprinted with permission from S. Waki, K. Hata, H. Sato, and Y. Saito, *J. Vac. Sci. Technol., B* **25** (2007) 517. Copyright 2007, American Vacuum Society.)

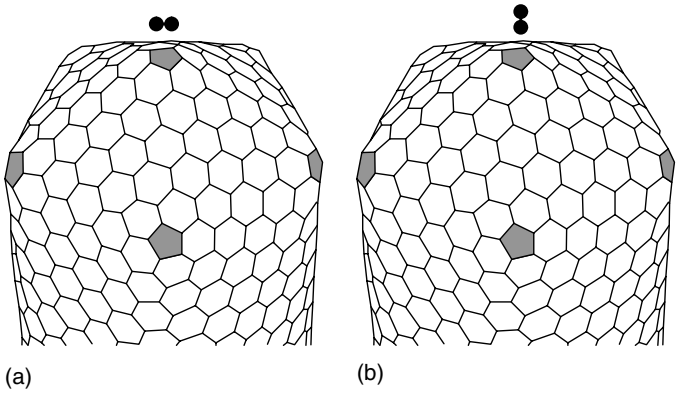

Figure 8.5 Model explaining two different adsorption states of a single nitrogen molecule. The molecular axis (a) parallel and (b) perpendicular to the substrate.

when the current is small, whereas it is a bright circular spot (Figure 8.4c) when the emission current is large. A model explaining two different adsorption states of a single nitrogen molecule is shown in Figure 8.5. If the molecular axis of nitrogen is parallel to the substrate, as illustrated in Figure 8.5a, the cocoon shape reflecting the shape of the molecule (interatomic distance of N_2 is 0.1094 nm) would be expected. When the molecular axis is perpendicular to the substrate (Figure 8.5b), on the other hand, the emission pattern should be a circular bright spot. In the latter configuration, the extended protrusion enhances the field concentration and thus brings about the enhanced emission current, that is, a brighter spot. The perpendicular configuration of the molecule is expected to gain larger adsorption energy than the parallel configuration because a larger polarization force is induced in the perpendicular configuration.

8.3.1.3 Oxygen

Exposure of an MWNT emitter to oxygen (1×10^{-8} Torr) brings about frequent adsorption and desorption phenomena at the pentagon sites [17], which is similar to the case of hydrogen and nitrogen, but the pentagonal rings do not recover after the disappearance of the bright spots. This suggests that pentagons are damaged during electron emission in the oxygen atmosphere. After the FE experiment in the oxygen atmosphere for 10 min, the MWNT emitter was heated (flashing at 1000 °C for 1 minute) again in an ultrahigh vacuum in order to desorb the oxygen molecules. All the pentagons were damaged, and the original pattern was no longer reproduced, exhibiting the very high reactivity of oxygen with the CNT surfaces.

8.3.1.4 Carbon Monoxide

When carbon monoxide was introduced into the FEM chamber up to pressure of 1.3×10^{-6} Pa, large bright spots corresponding to adsorption of the molecules appeared [17]. Even though the common flash-cleaning was applied to the emitter in ultrahigh vacuum after the electron emission for 600 s, the bright spot on the top pentagon did not disappear, and the clean pentagon pattern was not recovered. This suggests that the carbon monoxide molecule was strongly bonding to the pentagon, or it damaged the pentagon during the FE or flashing process.

8.3.1.5 Carbon Dioxide

FEM images of a single CO_2 molecule adsorbed on a MWNT also exhibited a cocoon-shaped bright spot as in Figure 8.6 [19]. Even though the CO_2 molecule is triatomic, it appears diatomic similar to a nitrogen molecule shown in the previous section. The reason for exhibiting the cocoon shape is probably the electric charge distribution within a CO_2 molecule, in which valence electrons lean toward the outer oxygen atoms from the central carbon atom.

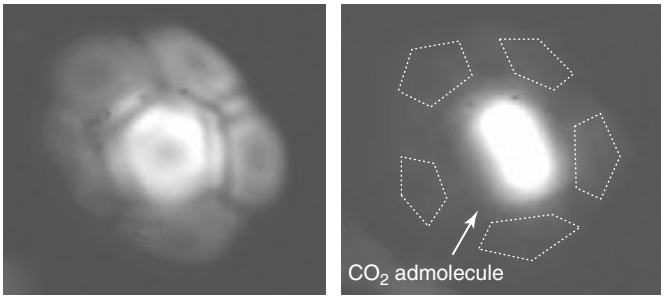

Figure 8.6 FEM images of (a) a clean MWNT tip and (b) a single CO_2 adsorbed on it. The CO_2 molecule exhibits a cocoon shape whose orientation changes randomly among the five discrete directions. (Reprinted with permission from Y. Kishimoto and K. Hata, *Surf. Interface Anal.* **40** (2008) 1669. Copyright 2008, Wiley.)

Though the CO_2 admolecule in Figure 8.6 moved randomly and discretely on the substrate pentagon with a time interval on the order of 100 ms, the orientation of the long axis of the admolecule is found to be arranged statistically equally into five groups, suggesting the presence of five equivalent, stable adsorption sites (orientations) for a CO_2 molecule on the pentagon. The angles between the molecular axes of the adjacent orientations are on average 36° with a slight deviation of only a few degrees, which is in good agreement with the angle expected for the symmetry of the pentagon. The length of the diagonal lines for the carbon pentagon with a side length of 0.142 nm, that is, C—C bond length of graphite, is 0.230 nm. This length is in good agreement with the distance between the two end oxygen atoms in the CO_2 molecule, that is, 0.233 nm. Details of the adsorption sites and the motion of CO_2 on the carbon pentagon are discussed in [19], in which the rotation angle of 72°, instead of 36°, is estimated from an analysis of the motion in the video file from frame to frame (time interval of 1/30 s) and also the rotation of the molecules around the central carbon atom is suggested.

8.3.1.6 **Methane**

Investigation of the effect of electric field on methane adsorption has revealed that methane adsorption occurs only when a negative electric voltage is applied to the emitter (i.e., being biased to emit electrons), whereas no methane adsorption is observed when a positive voltage or no voltage is applied in an atmosphere of 1.0×10^{-7} Pa methane gas [20].

FEM images of adsorbed methane molecules are usually simple, bright spots like in the case of inorganic molecules such as H_2, O_2, and CO mentioned above. Occasionally, however, a cross-shaped image is observed as shown in Figure 8.7. Since a CH_4 molecule has the tetrahedral structure, it looks like a ''cross'' when its twofold symmetry axis is normal to the substrate. The size of the cross image is roughly measured to be 0.23 nm on the basis of the size of a carbon pentagon, which was observed under the admolecule. Compared with the size of CH_4 (0.21 nm, the distance between two hydrogen atoms of a methane molecule), the FEM gives

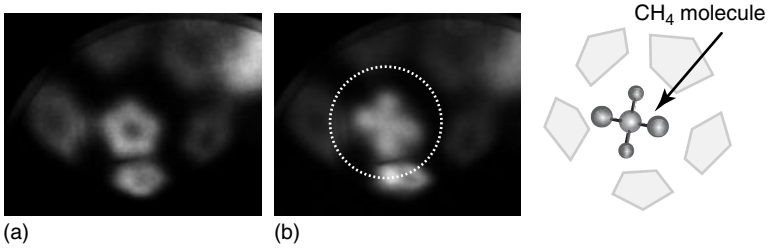

Figure 8.7 FEM images of (a) before and (b) after adsorption of a methane molecule on a pentagon at the MWNT tip. A cross-shaped image, reminiscent of a CH_4 molecule looked along the twofold rotational symmetry axis, is observed in (b).

a little larger image than the real size. This is presumably due to the enhanced magnification of a small protrusion on the round emitter surface [15]. From the shape and the size of the image, we may assume that the pattern corresponds to a single molecule of methane.

8.3.1.7 Comparison with Related Theoretical Studies

Theoretical calculations of FEM images of clean MWNT tips have been reported by Han and Ihm [21] and Khazaei *et al.* [22]. A brief explanation of the theories is given in Chapter 4. However, any theoretical studies that can be compared with FEM images of admolecules presented in this article or explain them are not available, whereas the variations of emission current due to adsorption of some molecules are discussed theoretically. According to Wadhawan *et al.* [23], adsorption of common electronegative gases, for example, O_2 and NH_3, can decrease the current, and inert gases such as He and Ar hardly affect the FE current and its stability. This theoretical prediction contradicts the experimental observations at least for the O_2 adsorption. Park *et al.* [24] ascribed the experimentally observed emission increase by oxygen adsorption to the local enhancement of electric field and the creation of new electronic states.

Li and Wang [25] predicted that the adsorption of CO and CH_4 decrease the emission current because of an increase in the work function. Sheng *et al.* [26], on the other hand, predicted that CO and CO_2 decrease the current, but CH_4 increases it. Contradictions between the theoretical works themselves are found. Experimentally, all kinds of molecules have been shown to bring about emission enhancement upon their adsorption on a CNT.

8.3.2 Aluminum Clusters

Figure 8.8a shows a transmission electron microscope (TEM) picture of Al with a mean thickness of 2.5 nm deposited on MWNTs before the FE experiment. The deposited Al formed a discontinuous film consisting of isolated islands with the diameter of a few nanometers. After the FE experiment, diameter of the Al clusters increased to about 10 nm as revealed in Figure 8.8b.

During the study on the effect of Al deposition on FE properties, intriguing FEM images suggestive of an Al cluster with atomic resolution were observed [27]. Figure 8.9a and b shows the FEM images of an MWNT emitter before and after Al deposition, respectively. A spotty pattern with high symmetry (fourfold symmetry in this case) appeared on the pentagon patterns characteristic of the clean caps of MWNTs (two MWNTs are visible in Figure 8.9a) after the Al deposition, as shown in Figure 8.9b. The contrast of the spotty pattern is reminiscent of the structure of an atom cluster with the shape of cubo-octahedron, which is a crystal form characteristic of face-centered cubic (fcc) metals [28]. A model of the structure consisting of 38 Al atoms is illustrated in Figure 8.10. The fourfold symmetry of the Al image suggests that the Al cluster is oriented with its [100] direction normal to the nanotube surface. Four bright spots observed in the central part of the Al

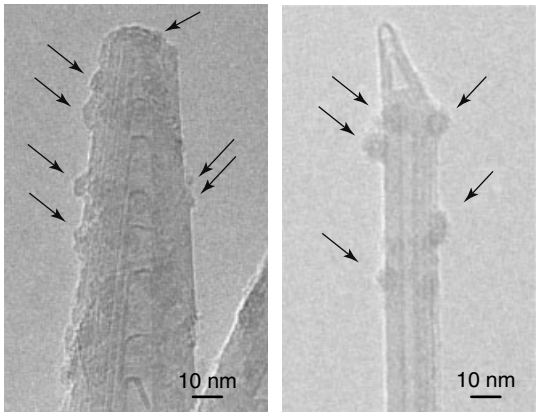

Figure 8.8 TEM images of Al-deposited MWNTs (a) before and (b) after field emission. Mean thickness of the deposited Al is 2.5 nm. Arrows indicate Al clusters. Different MWCNTs are shown in (a) and (b).

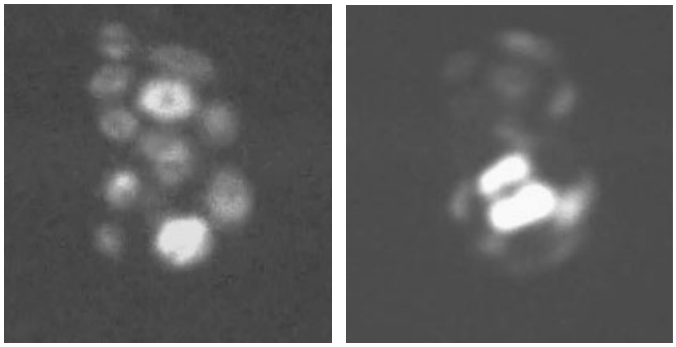

Figure 8.9 FEM images of (a) clean MWNT caps and (b) an Al cluster on a MWNT tip.

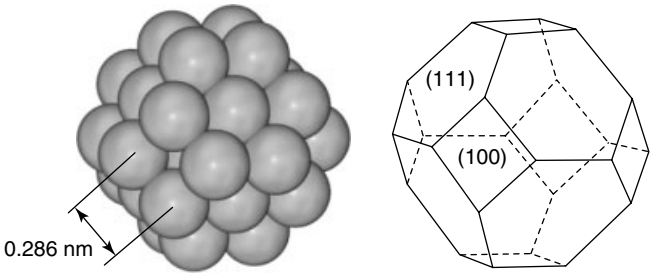

Figure 8.10 Cubo-octahedron of an Al_{38} cluster.

image correspond to the four corners of the top (100) surface. Four dark regions surrounding the central (100) face correspond to (111) faces, which are outlined by bright edges and corners.

The distance between neighboring atoms along the edge of the (100) surface is 0.286 nm when the lattice constant of the cluster is the same as that of bulk Al. Using the size of the carbon pentagon (approximately 0.25 nm in diameter) as a measure of the magnification of FEM images (under the assumption that the pentagon image originates from five carbon atoms comprising a pentagon), the distance between the bright spots at the corners of the (100) face is roughly estimated to be in the range of 0.30 nm, which is a little larger than the nearest neighbor distance on the Al (100) surface due to the local magnification enhancement by a small protrusion on a round tip.

Metal clusters or nanoparticles often exhibit atomic structures different from crystal structures in bulk, for example, icosahedral or multiply twinned structures for elements that form fcc structures in bulk. For Al, however, icosahedral structures have never been observed even for small particles by electron microscopy [28]. Theoretical calculations also suggest that the structural transition from the fcc to the icosahedral structures lies in a range of size between 13 and 55 atom clusters [29]. The present Al cluster falls in this transition range in size. Thus, it is highly probable that the Al cluster exhibits the same structure as the bulk.

The polyhedral Al cluster (Figure 8.9b), which exhibits rotation and migration, disappeared in several seconds from the field of view after its appearance, and finally the original clean cap was recovered. The migration and diffusion of Al clusters on MWNTs are responsible for the increased diameter of Al clusters observed by TEM after the FE experiment, as shown in Figure 8.8b.

8.4
Resolution in FEM and Possible Observation of Atomic Detail

In 1956, Rose [15] gave the equation of FEM resolution δ, which consists of two principal components, namely, the momentum uncertainty and the effect of the transverse velocities of the electrons near the top of Fermi level in the emitter:

$$\delta = \left(\frac{2\hbar\tau}{mM}\right)^{1/2}\left(1 + \frac{2m\tau v_0^2}{\hbar M}\right)^{1/2} \tag{8.1}$$

where M is the magnification, τ is the time of flight of an electron from the emission tip to the screen, v_0 is the average transverse velocity, $\hbar$ is the Planck constant/2π, and m is the electron mass. When M/τ is large enough to assume $2m\tau v_0^2/\hbar M \ll 1$, the term containing v_0 becomes negligible and the resolution is limited by the uncertainty principle. Under such a condition, say $M/\tau \approx 2.5 \times 10^{15}$, he suggested that small protrusions on the surface of the tip can provide resolutions on the order of 0.3 nm so that some of their atomic detail should be observable. M is always reduced by a factor β from that expected for a spherically symmetric geometry

where the tip and screen are assumed to be concentric spheres of radii R and z, that is,

$$M = z/\beta R \tag{8.2}$$

Using the approximation $\beta \approx 1.9$, $\tau \approx z\,(2eV/m)^{-1/2}$, and $v_0 \approx 2 \times 10^5 \mathrm{ms}^{-1}$ ($= 0.11$ eV), the following practical form of solution equation [15, 16] is obtained:

$$\delta = 0.860 \left(\frac{R}{\sqrt{V}}\right)^{\frac{1}{2}} \left(\frac{1 + 2.22R}{\sqrt{V}}\right)^{\frac{1}{2}} \tag{8.3}$$

where δ is in nanometers, R is the tip radius in nanometers, and V is the applied potential in volts between the tip and the screen.

From Eq. (8.3), we see that atomic resolution is attainable for $R/\sqrt{V} \prec 1$. In an experiment using the MWNT as the emitter, R and V are about 5 nm and 1.5 kV, respectively. These parameters give a resolution on the order of 0.3 nm, indicating that some of atomic detail is observable in the present experimental condition.

8.5 Concluding Remarks

CNTs possess unique structural and physicochemical properties distinct from traditional metal emitters (e.g., tungsten and molybdenum): extremely small tip radius (1–10 nm); well-defined, stable surface structures (composed of carbon hexagons and pentagons) made of strong C–C bonds; no oxide formation and no surface diffusion of carbon atoms. This chapter reviews recent FEM studies that suggest near-atomic resolution images of molecules and metal clusters adsorbed CNT emitters. The high resolution is probably due to the small tip radius of CNT emitters as suggested by the Rose's estimation of resolution [15] – though it is rather old. Appearance of pentagons in FEM images as a measure of magnification of the images is another merit of CNT emitters. Adsorbed molecules shown in this chapter are common, small molecules such as N_2 and CO. When metal (W or Mo) needles were employed as the FEM emitter, such molecular images reflecting their structures were never observed because of the presumable reactions between the admolecule and the metal surface. Chemical inertness of CNT surfaces is responsible for the stable observation of these small molecules.

In the 1950s, there was controversy as to whether objects of atomic dimensions can be resolved by FEM. The most interesting and yet controversial FEM patterns are quadruplet or doublet patterns originating from organic dye molecules such as phthalocyanine or flavanthrene reported first by Müller [30]. The advent of CNTs as field emitters will revive the discussion on FEM resolution and open a new scene in the FEM technique for direct observation of adatoms and admolecules. For developing the FEM technique, a realistic theory applicable to CNT emitters is

highly required since the simple FN theory is inadequate for more sophisticated analyses of FEM observations.

References

1. Gadzuk, J.W. and Plummer, E.W. (1973) *Rev. Mod. Phys.*, **45**, 487.
2. Melmed, A.J. and Müller, E. (1958) *J. Chem. Phys.*, **29**, 1037.
3. Gomer, R. (1961) *Field Emission and Field Ionization*, Harvard University Press, Cambridge.
4. Demczyk, B.G., Wang, Y.M., Cumings, J., Hetman, M., Han, W., Zettl, A., and Ritchie, R.O. (2002) *Mater. Sci. Eng. A*, **334**, 173.
5. Wei, B.Q., Vajtai, R., and Ajayan, P.M. (2001) *Appl. Phys. Lett.*, **79**, 1172.
6. Nakayama, Y., Nishijima, H., Akita, S., Hohmura, K.I., Yosimura, S.H., and Takeyasu, K. (2000) *J. Vac. Sci. Technol., B*, **18**, 611.
7. Saito, Y., Seko, K., and Kinoshita, J. (2005) *Diamond Relat. Mater.*, **14**, 1843.
8. Saito, Y., Hamaguchi, K., Hata, K., Tohji, K., Kasuya, A., Nishina, Y., Uchida, K., Tasaka, Y., Ikazaki, F., and Yumura, M. (1998) *Ultramicroscopy*, **73**, 1.
9. Hata, K., Takakura, A., and Saito, Y. (2001) *Surf. Sci.*, **490**, 296.
10. Tamura, R. and Tsukada, M. (1995) *Phys. Rev. B*, **52**, 6015.
11. Yamamoto, S., Hosoki, S., Fukuhara, S., and Futamoto, M. (1979) *Surf. Sci.*, **86**, 734.
12. Ishizawa, Y., Aizawa, T., and Otani, S. (1993) *Appl. Surf. Sci.*, **67**, 36.
13. Saito, Y., Hamaguchi, K., Hata, K., Uchida, K., Tasaka, Y., Ikazaki, F., Yumura, M., Kasuya, A., and Nishina, Y. (1997) *Nature*, **389**, 554.
14. Saito, Y., Tsujimoto, Y., Koshio, A., and Kokai, F. (2007) *Appl. Phys. Lett.*, **90**, 213108.
15. Rose, D.R. (1956) *J. Appl. Phys.*, **27**, 215.
16. Brodie, I. (1978) *Surf. Sci.*, **70**, 186.
17. Hata, K., Takakura, A., and Saito, Y. (2003) *Ultramicroscopy*, **95**, 107.
18. Waki, S., Hata, K., Sato, H., and Saito, Y. (2007) *J. Vac. Sci. Technol., B*, **25**, 517.
19. Kishimoto, Y. and Hata, K. (2008) *Surf. Interface Anal.*, **40**, 1669.
20. Yamashita, T., Asaka, K. Nakahara, H., and Saito, Y. (2008) Presented at the 7th International Vacuum Electron Sources Conference (IVESC 2008), Queen Mary, University of London, August 4-6, 2008, London .
21. Han, S. and Ihm, J. (2002) *Phys. Rev. B*, **66**, 241402 (241(R)).
22. Khazaei, M., Farajian, A.A., and Kawazoe, Y. (2005) *Phys. Rev. Lett.*, **95**, 177602.
23. Wadhawan, A., Stallcup, R.E.II, Stephens, K.F.II, Perez, J.M., and Akwani, I.A. (2001) *Appl. Phys. Lett.*, **79**, 1867.
24. Park, N., Han, S., and Ihm, J. (2001) *Phys. Rev. B*, **64**, 125401.
25. Li, Z. and Wang, C.-Y. (2006) *Chem. Phys.*, **330**, 417.
26. Sheng, L.M., Liu, P., Liu, Y.M., Qian, L., Huang, Y.S., Liu, L., and Fan, S.S. (2003) *J. Vac. Sci. Technol., A*, **21**, 1202.
27. Saito, Y., Matsukawa, T., Yamashita, T., Asaka, K., Nakahara, H., and Uemura, S. (2007) Presented at the 14th International Display Workshops (IDW'07), Sapporo Convention Center Sapporo Japan, December 5-7, 2007.
28. Kimoto, K. and Nishida, I. (1977) *Jpn. J. Appl. Phys.*, **16**, 941.
29. Cheng, H.P., Berry, R.S., and Whetten, R.L. (1991) *Phys. Rev. B*, **43**, 10647.
30. Müller, E.W. (1950) *Z. Naturforsh.*, **5a**, 473.

9
In situ Transmission Electron Microscopy of CNT Emitters

Koji Asaka and Yahachi Saito

9.1
Introduction

Since the first experiments demonstrating the excellent electron field emission properties of carbon nanotubes [1, 2], various emitter devices such as flat panel displays, cathode ray tubes, miniature X-ray tubes, microwave devices, and electron sources for electron microscopes have been developed. For the optimization of their performance, it is important to examine directly the behavior of individual nanotube emitters in electric fields and to understand the electron field emission properties since the emission properties depend on the structural and electronic features that are intrinsic to the individual nanotubes as well as configurations between the emitter and a counter electrode. The structural behavior and emission properties of individual multiwall carbon nanotubes (MWNTs) in electric fields have been investigated by scanning electron microscopy (SEM). Wei *et al.* demonstrated that MWNTs with a curved shape, prepared by thermal decomposition of CH_4 and H_2, were oriented parallel to the electric field line under an applied electric field, and then recovered the initial shape after the electric field was removed [3]. A decrease of the length of the MWNTs after field emission at currents of 50–120 nA for 30 min was also observed. Bonard *et al.* observed the degradation and failure of the individual MWNTs after field emission [4]. They also suggested that only a small number of exceptionally long and/or narrow nanotubes contribute to the emission current in large area measurements using nanotube films [5]. However, SEM is not suitable for *in situ* observations of the structural behavior of the individual nanotubes during field emission because the large number of electrons emitted form the nanotubes surpasses the number of signal electrons and saturates the electron detector of the microscope. Alternatively, experimental methods to manipulate the individual nanotubes in a transmission electron microscope and to measure the *in situ* field emission properties with simultaneous imaging have been developed. *In situ* transmission electron microscopy (TEM) possesses the advantage that it is possible to observe the structural dynamics of the individual nanotubes during field emission at a higher spatial resolution. Here, *in situ* TEM studies of the carbon nanotube emitters are described.

Carbon Nanotube and Related Field Emitters: Fundamentals and Applications. Edited by Yahachi Saito

ISBN: 978-3-527-32734-8

9.2
Degradation and Failure of Nanotubes at Large Emission Current Conditions

Pioneering studies of the *in situ* observations of nanotubes in electric fields by TEM have been reported by Wang *et al.* [6, 7]. They observed two types of structural damages: that is, ''splitting'' and ''stripping'' of MWNTs under applied high electric field conditions sufficient to extract large emission currents. Figure 9.1 shows a time-sequence series of images of the splitting process of an MWNT during field emission. The diameter of the MWNT, which was produced by the arc-discharge technique, is ~20 nm. The gap from the MWNT tip to the counter electrode used as anode is ~2 μm. The emission current increases from 10 to 250 μA as the applied voltage between the MWNT tip and the anode increases from 80 to 130 V. At 90 V, the emission current increases to 40 μA and the walls of the MWNT split, as shown in Figure 9.1b. They suggested that the mechanism of the damage is the electrostatic force acting on the MWNT tip. The splitting damage is accompanied by an abrupt increase in the emission current during field emission [8, 9]. A stripping structural damage of MWNTs during field emission was observed at a gap width of ~2 μm at applied voltages from 100 to 200 V. The wall of the MWNT was degraded and decreases in diameter and length occurred in the MWNT. During

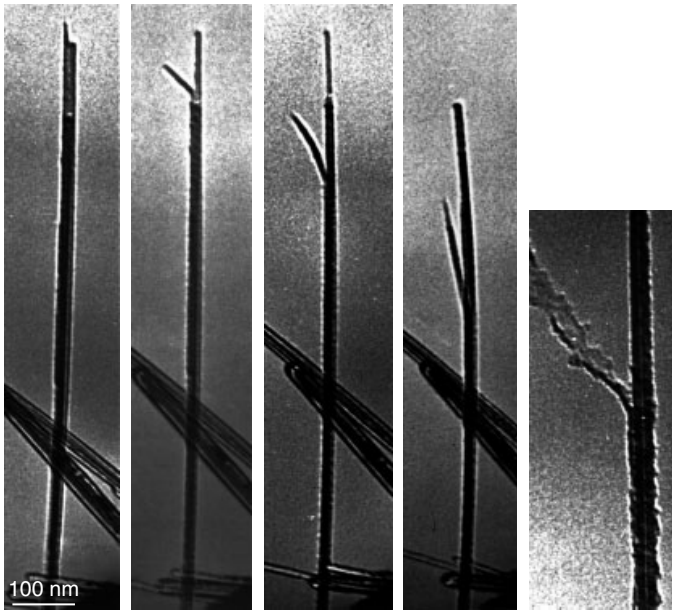

Figure 9.1 Time-sequence series of images of the ''splitting'' process of an MWNT during field emission. (Reproduced with permission from Z.L. Wang *et al.*, *Appl. Phys. Lett.*, **80**, 856 (2002).)

the degradation process, a decrease of the emission current was also observed [9]. Similar degradation processes of doublewall carbon nanotubes (DWNTs) during field emission were reported by Saito *et al.* [10]. Figure 9.2 shows a time-sequence series of images of the degradation process of DWNT bundles during field emission at applied voltages from 50 to 100 V. In Figure 9.2a, the dark regions at the top and bottom are the surfaces of a tungsten needle attached to the DWNTs and of a copper plate used as anode, respectively. The gap width before the field emission experiment is ~2 μm. The most protruding DWNT bundle A is split at an applied

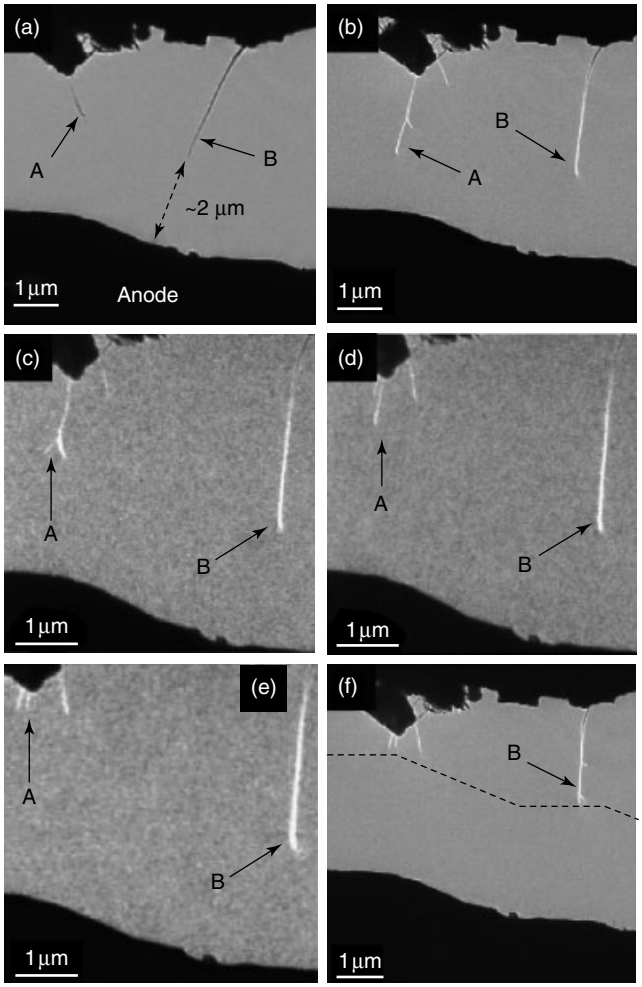

Figure 9.2 Time-sequence series of images of the degradation process of DWNT bundles during field emission. (Reproduced with permission from Y. Saito *et al.*, *Diamond Relat. Mater.*, **14**, 1843 (2005).)

voltage of 60 V (Figure 9.2b) and gradually sublimated between 60 and 85 V, which results in a decrease in the length (Figure 9.2c–e). After the decrease in length of the bundle, the degradation proceeds to the next protruding bundle B. Finally, the degradation ceases when the distances between the bundle tips and the anode surface become uniform (Figure 9.2f). As one cause of the degradation, such as the decrease in length at large emission currents, sublimation by Joule resistive heating was proposed.

Wei *et al*. proposed that the temperature during field emission is highest at the interior rather than the tip of a carbon nanotube on the basis of the one-dimensional heat equation considering the cooling effect due to electron emission and showed by *in situ* TEM that the nanotubes during field emission collapsed at the point close to the highest temperature [11].

Jin *et al*. demonstrated that a single MWNT with 15 nm diameter was capable of emitting large emission currents up to ~26 μA, but after 10 min the emission current suddenly reduced to zero, resulting from the fatal structure damage [12].

9.3 Effect of Tip Structure of Nanotubes on Field Emission

The structures and the surface conditions of the nanotube tip influence field emission properties [12–16]. Wang *et al*. modified the tip structure of MWNTs by controlled field-induced evaporation and measured the field emission properties *in situ* [15]. Figure 9.3a–d shows images of an MWNT tip structure after the modification by field evaporation. The diameter and length of the MWNT are ~10 and 315 nm, respectively. The MWNT in Figure 9.3a has a sharp tip structure. After applying a few voltage scans with a sweeping time of 200 ms, the sharp tip is modified into a blunt one, as shown in Figure 9.3b–d. The emission current leading to evaporation is several tens of microamperes. Figure 9.3e and f shows the current–voltage curves during field emission and their Fowler–Nordheim plots for the MWNT in Figure 9.3a–d, respectively. The gap width is 380 nm. The applied voltage required for start of the emission of the current increases from 19 to 42 V (a–d in Figure 9.3e) as the sharp tip is transformed into a hemispherical one (Figure 9.3a–d). From the slope of the Fowler–Nordheim plots, the corresponding field conversion factors of the MWNTs in Figure 9.3a–d were estimated to be 1/4.6, 1/5.6, 1/6.5, and 1/9.5 nm^{-1}, respectively. The *in situ* observation shows experimentally that the factors decrease with the increase in the radius of curvature of the nanotube tip using the same MWNT. In addition, they observed that the cap of an MWNT with ~37 nm diameter was opened by field evaporation, and examined *in situ* the field emission properties at a gap width of 660 nm. They showed that the field emission easily occurs in an open-ended MWNT rather than in a capped one at a low applied voltage.

Xu *et al*. measured the work function of MWNTs with various tip structures by *in situ* TEM and demonstrated that the work function at the MWNT tips sensitively changed depending on its tip structures and surface conditions [13]. The field

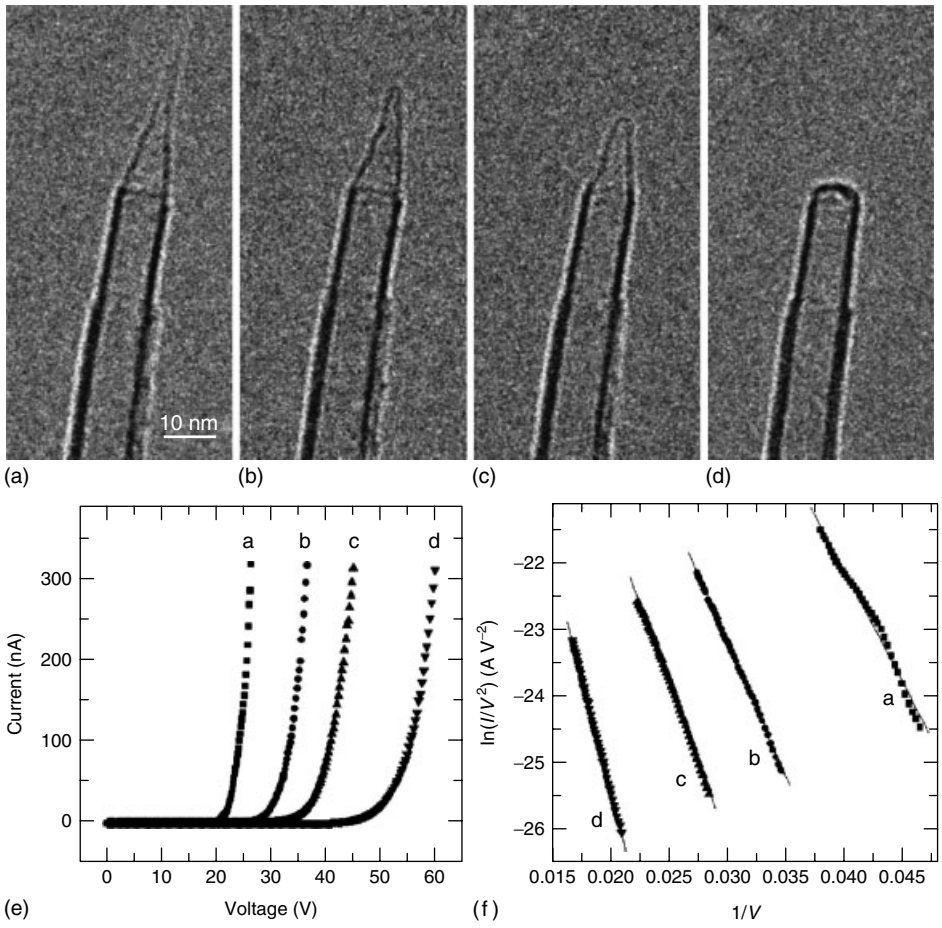

Figure 9.3 (a–d) Images of a MWNT tip structure after the modification by field evaporation. (e) and (f) Current–voltage curves during field emission and their Fowler–Nordheim plots for the MWNT in (a–d), respectively. (Reproduced with permission from M.S. Wang *et al.*, *Appl. Phys. Lett.*, **88**, 243108 (2006).)

conversion factor and the work function are essential parameters that determine the field emission properties. Their precise quantification is important for the evaluation of the field emission properties of nanotube emitters.

9.4
Relationship between Field Emission and Gap Width

The gap width between the nanotube tip and the counter anode is one of the crucial factors to evaluate field emission characteristics. Asaka *et al.* fabricated a

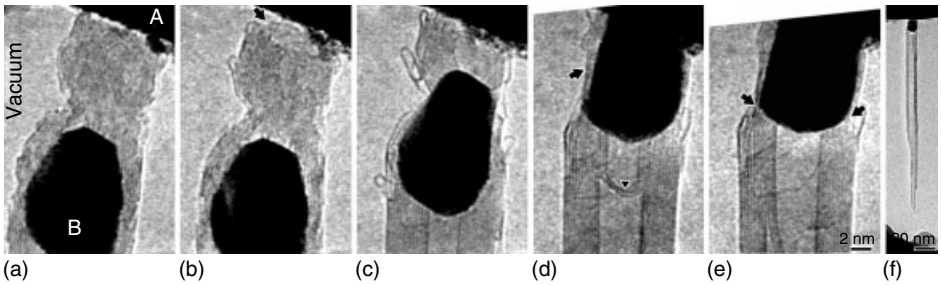

Figure 9.4 Time-sequential series of high-resolution images of the welding process of a MWNT to the metal surface. The tip diameter and length of the MWNT emitter are 5 and 176 nm, respectively, as shown in (f). The MWNT tip is closed. (Reproduced with permission from K. Asaka *et al.*, *Appl. Phys. Lett.*, **92**, 023114 (2008).)

single MWNT emitter on a metal surface by welding in a transmission electron microscope and examined *in situ* the field emission properties at various gap widths [17]. Figure 9.4a–e shows a time-sequential series of high-resolution images of the welding process of an MWNT to the metal surface. In Figure 9.4a, the dark regions at the top A and bottom B are the platinum surface and a platinum particle encapsulated in the MWNT, respectively. In this welding process, each layer consisting of the MWNT is directly connected to the particle at the junction between the MWNT and the particle, as shown by two small arrows in Figure 9.4e, suggesting that an ohmic contact forms at the junction. After welding, the single MWNT emitter is formed on the platinum surface, as shown in Figure 9.4f. The tip diameter and length of the MWNT are 5 and 176 nm, respectively. The nanotube tip is closed. In Figure 9.4f, the dark region at the bottom is a copper plate used as the anode. Figure 9.5a shows the current–voltage curves during field emission at gap widths in the range from 27 to 442 nm. The applied voltage required for an emission current of 100 nA increases with the increase of the gap from 27 to 442 nm. At 27 nm, the emission current starts to be observed at only 29 V and increases up to 14 μA at 42 V. Figure 9.5b shows the Fowler–Nordheim plots obtained from the current–voltage curves in Figure 9.5a. From the slope of these plots, the field enhancement factors (βs) are estimated and presented as a function of the gap width (d) in Figure 9.5c. The field enhancement factors decrease with decreasing gap width, and it is well approximated by $\beta = 1 + d^{0.79}$. The decrease results from an approximately parallel plate configuration of the nanotube tip and the anode, as reported previously [18].

9.5 Other Studies by *In situ* TEM of CNT Emitters

Comings *et al.* performed electron holography experiments of individual field-emitting MWNTs inside a transmission electron microscope and examined the

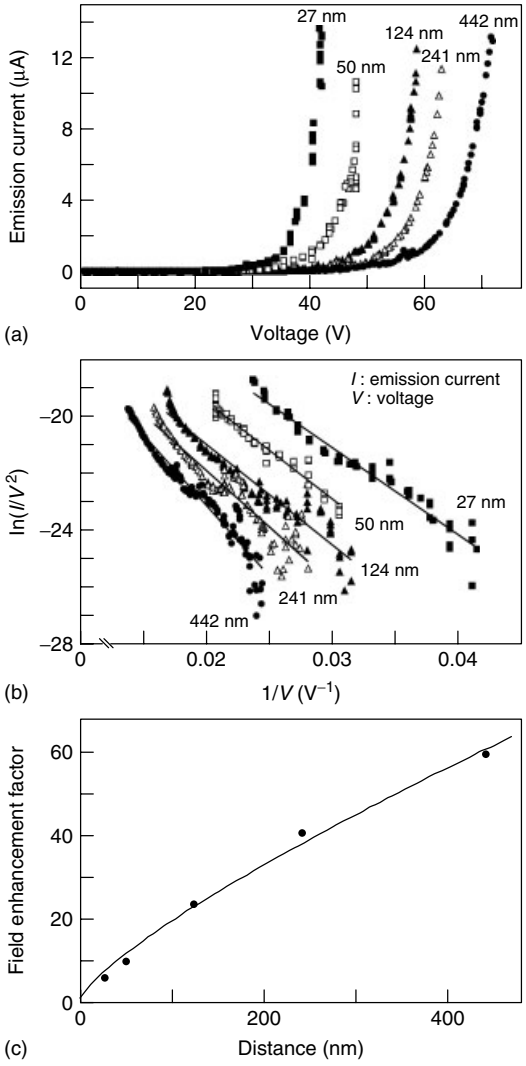

Figure 9.5 (a) Current–voltage curves during field emission at gap widths of 27–442 nm. (b) Fowler–Nordheim plots obtained from the current–voltage curves in (a). (c) Field enhancement factors as a function of the gap distance. Dots represent experimental data, and the solid curve shows a fitting curve, $\beta = 1 + d^{0.79}$. (Reproduced with permission from K. Asaka *et al.*, *Appl. Phys. Lett.*, **92**, 023114 (2008).)

magnitude and spatial distribution of the electric field surrounding the MWNT [19]. They revealed that the field strength was highest at the tip of the MWNT and not at the sidewall defects. They also showed that individual MWNTs can be used as a nanoscale electrostatic biprism for electron holography [20].

Gao *et al.* measured by *in situ* TEM the work function at the tips of individual MWNTs with diameters of 14–55 nm [21]. The majority (70%) of investigated

MWNTs gave work functions in the range 4.6–4.8 eV, which falls in the range of previously reported values for graphite materials [22]. The other MWNTs had a work function of ~6.5 eV. They suggested that the discrepancy might be due to the metallic and semiconductive characteristics of the MWNTs.

References

1. de Heer, W.A., Châtelain, A., and Ugarte, D. (1995) A carbon nanotube field-emission electron source. *Nature*, **270**, 1179–1180.
2. Rinzler, A.G., Hafner, J.H., Nilolaev, P., Lou, L., Kim, S.G., Tománek, D., Nordlander, P., Colbert, D.T., and Smalley, R.E. (1995) Unraveling nanotubes: field emission from an atomic wire. *Science*, **269**, 1550–1553.
3. Wei, Y., Xie, C., Dean, K.A., and Coll, B.F. (2001) Stability of carbon nanotubes under electric field studied by scanning electron microscopy. *Appl. Phys. Lett.*, **79**, 4527–4529.
4. Bonard, J.-M., Klinke, C., Dean, K.A., and Coll, B.F. (2003) Degradation and failure of carbon nanotube field emitters. *Phys. Rev. B*, **67**, 115406-1–115406-10.
5. Bonard, J.-M., Dean, K.A., Coll, B.F., and Klinke, C. (2002) Field emission of individual carbon nanotubes in the scanning electron microscope. *Phys. Rev. Lett.*, **89**, 197602-1–197602-4.
6. Wang, Z.L., Poncharal, P., and de Heer, W.A. (2000) Nanomeasurements in transmission electron microscopy. *Microsc. Microanal.*, **6**, 224–230.
7. Wang, Z.L., Gao, R.P., de Heer, W.A., and Poncharal, P. (2002) In situ imaging of field emission from individual carbon nanotubes and their structural damage. *Appl. Phys. Lett.*, **80**, 856–858.
8. Fujieda, T., Hidaka, K., Hayashibara, M., Kamino, T., Matsumoto, H., Ose, Y., Abe, H., Shimizu, T., and Tokumoto, H. (2004) In situ observation of field emissions from an individual carbon nanotube by Lorentz microscopy. *Appl. Phys. Lett.*, **85**, 5739–5741.
9. Doytcheva, M., Kaiser, M., and de Jonge, N. (2006) In situ transmission electron microscopy investigation of the structural changes in carbon nanotubes during electron emission at high currents. *Nanotechnology*, **17**, 3226–3233.
10. Saito, Y., Seko, K., and Kinoshita, J. (2005) Dynamic behavior of carbon nanotube field emitters observed by in situ transmission electron microscopy. *Diamond Relat. Mater.*, **14**, 1843–1847.
11. Wei, W., Liu, Y., Wei, Y., Jiang, K., Peng, L.-M., and Fan, S. (2007) Tip cooling effect and failure mechanism of field-emitting carbon nanotubes. *Nano Lett.*, **7**, 64–68.
12. Jin, C., Wang, J., Wang, M., Su, J., and Peng, L.-M. (2005) In-situ studies of electron field emission of single carbon nanotubes inside the TEM. *Carbon*, **43**, 1026–1031.
13. Xu, Z., Bai, X.D., Wang, E.G., and Wang, Z.L. (2005) Field emission of individual carbon nanotube with in situ tip image and real work function. *Appl. Phys. Lett.*, **87**, 163106-1–163106-3.
14. Wang, M.S., Peng, L.-M., Wang, J.Y., and Chen, Q. (2005) Electron field emission characteristics and field evaporation of a single carbon nanotube. *J. Phys. Chem. B*, **109**, 110–113.
15. Wang, M.S., Wang, J.Y., and Peng, L.-M. (2006) Engineering the cap structure of individual carbon nanotubes and corresponding electron field emission characteristics. *Appl. Phys. Lett.*, **88**, 243108-1–243108-3.
16. Kaiser, M., Doytcheva, M., Verheijen, M., and de Jonge, N. (2006) In situ transmission electron microscopy observation of individually selected freestanding carbon nanotubes during field emission. *Ultramicroscopy*, **106**, 902–908.
17. Asaka, K., Nakahara, H., and Saito, Y. (2008) Nanowelding of a multi-walled carbon nanotube to metal

surface and its electron field emission properties. *Appl. Phys. Lett.*, **92**, 023114-1–023114-3.

18. Smith, R.C., Cox, D.C., and Silva, S.R.P. (2005) Electron field emission from a single carbon nanotube: effects of anode location. *Appl. Phys. Lett.*, **87**, 103112-1–103112-3.

19. Cumings, J., Zettl, A., McCartney, M.R., and Spence, J.C.H. (2002) Electron holography of field-emitting carbon nanotubes. *Phys. Rev. Lett.*, **88**, 056804-1–056804-4.

20. Cumings, J., Zettl, A., and McCartney, M.R. (2004) Carbon nanotube electrostatic biprism: principle of operation and proof of concept. *Microsc. Microanal.*, **10**, 420–424.

21. Gao, R., Pan, Z., and Wang, Z.L. (2001) Work function at the tips of multiwalled carbon nanotubes. *Appl. Phys. Lett.*, **78**, 1757–1759.

22. Weast, R.C. (1976–1977) *Handbook of Chemistry and Physics*, 5th edn, CRC Press, p. E-81.

10
Field Emission from Single-Wall Nanotubes

Kenneth A. Dean

10.1
Introduction

Single-wall nanotubes (SWNTs) provide the best field-emitting geometry known to humankind. They are routinely formed with diameters on the order of 1 nm and aspect ratios greater than 1000. From a chemical standpoint, their covalently bonded structures make them more robust than traditional metallic structures and immune from electromigration. Simply put, SWNTs make excellent electron emitters.

While SWNT emitters do follow the Fowler–Nordheim tunneling theory under the right conditions, the details of their emission behavior are far richer. The Fowler–Nordheim description was developed for metals, and it is applicable only for very specific surface conditions [1, 2]. SWNTs do not generally present these special surface conditions, and they readily operate outside the Fowler–Nordheim assumptions. The field emission behavior of SWNTs is dominated by surface states arising from both the nanotubes structures themselves and external molecular interactions. Moreover, the stability of nanotube field emitters provides readily observable phenomena that occur at temperature, current, and electric field conditions that are well beyond the destruction limit of other types of emitters.

Many of these behaviors affect the engineering designs of devices incorporating SWNT electron emitters. To promote the design and construction of SWNT field emission devices, this chapter summarizes the current understanding of SWNT field emission behavior over a broad range of operating conditions.

10.2
Single-Wall Nanotubes and Field Emission

SWNTs are typically grown from a seed catalyst nanoparticle by arc evaporation, laser evaporation, or chemical vapor deposition. Each technique produces a diverse

Carbon Nanotube and Related Field Emitters: Fundamentals and Applications. Edited by Yahachi Saito

ISBN: 978-3-527-32734-8

population of SWNTs, and the mixture often includes multiwalled nanotubes (MWNTs) and other carbon forms as well. Each technique produces a population of nanotubes with differences in diameter, length, chirality, and conductivity. Synthesized SWNTs range in diameter from approximately 0.5 to greater than 6 nm, with typical techniques producing nanotubes between 1 and 2 nm [3]. They typically range in length from a few nanometers to many micrometers. The chiral twist of SWNT graphitic sheet walls relative to the tube axis gives rise to a band structure such that approximately one-third of possible SWNT structures are metallic tubes while two-thirds are semiconducting tubes [4]. Of course, the population fractions of these tubes vary with the synthesis technique. SWNTs are also terminated by a cap, and each cap structure presents different electronic states for field emission. In short, SWNTs are not a homogenous material, but rather a population of structures with widely varying field emission properties.

10.3
Measuring the Properties of a Single SWNT

The majority of publications that characterize the field emission properties of nanotubes begin with nanotube films prepared on a flat surface. To use experimentally convenient voltages, the extraction electrode, which is typically a phosphor screen or small-diameter metallic probe, is positioned within 50–500 μm of the emitter surface [5, 6]. While these methods provide relevant information on current density and emitter uniformity, they lack the means to provide a detailed understanding of underlying emitter physics. For example, measuring a large ensemble of nanotubes with different cap structures, diameters, lengths, and conductivities produces a composite current–voltage curve heavily weighted to the behavior of emitters with the highest aspect ratio. Temporal behaviors are also washed out, as the behaviors of many nanotubes are averaged together. It is difficult to understand nanotube physics by studying samples with large numbers of emitters. Moreover, a parallel plate electrode geometry provides poor gas conductance, creating a local environment at the field emitter that is dominated by outgassing from electron-bombarded surfaces, rather than by the pressure of the measurement chamber. Under these conditions, the cleanliness of the field-emitting surface can neither be measured nor controlled, and this undermines the interpretation of any experimental results.

These experimental shortcomings can be overcome by employing traditional field emission microscopy techniques [7]. The electrodes are spaced far apart, providing controllable vacuum conditions. Moreover, the geometry magnifies the electron beam as much as a million times, allowing for real-time observation of the changes in the spatial variations of the electron current density across the emitting surface. The emitters themselves can be mounted on a heating element, allowing for surface modification and cleaning. The field emission microscope technique can control the relevant variables.

While the field emission microscopy technique is powerful, obtaining results from a single nanotube requires some technique in sample preparation. However, the exponential dependence of field emission current on nanotube geometry works in the scientist's favor. Given a population of nanotubes, only the sharpest few will emit, so a sample can contain many more nanotubes than emit. In addition, the field emission microscope geometry can image the emission from several nanotubes, and in many cases, the images are completely nonoverlapping. With these advantages, a number of investigators have been successfully preparing nanotube field emitters on a standard scanning electron microscope filament assembly by applying carbon paint to the filament as an adhesive, and gently touching the wet adhesive to powdered nanotubes. The adhesive picks up a sparse enough population of nanotubes to produce a sample with one emitting nanotube.

An experimental challenge with SWNTs is measuring the structure of the nanotube that is field emitting. Typically, individual SWNTs (as opposed to bundles of SWNTs) are too small to be observed and accurately measured by scanning electron microscopy, although their presence can be detected by transport measurements between two probes. While SWNTs are readily observed via transmission electron microscopy, the primary field emitters are typically micrometer-long, free-ended nanotubes. These vibrate in the microscope, causing blurring of the tube everywhere but at its anchor point. Distinct field-emitting SWNTs have rarely been structurally characterized.

Recently, Arnold *et al.* demonstrated a means for purifying and separating nanotubes by size and chirality [8]. This opens the possibility of measuring a known type of nanotube, based on pure starting material. To date, however, no such measurements have been reported.

10.4
Field Emission from a Clean SWNT Surface

Researchers have observed that nanotubes, like metals, emit electrons from adsorbate states unless the surface is cleaned properly [9]. In the vast majority of experimental situations, the adsorbate states dominate SWNT behavior, and this will be covered in Section 10.5. The pure behavior of the nanotube cap is obtained when the nanotube surface is cleaned properly.

Dean and Chalamala reported that SWNTs can be cleaned in an ultrahigh vacuum (UHV) field emission microscope by thermal desorption at 900 K under an applied field [10]. During the cleaning process, the field emission microscope image changed rapidly as adsorbates were thermally excited, but the image became stable and static once the surface was clean. When the sample temperature was returned to room temperature, the clean image remained the same, as long as the surface remained clean (minutes to hours). It should also be noted that the adsorbate states emitted 10–100 times more current than the clean nanotube surface, so the cleaning processes results in a significant decrease in electron current. This

cleaning process and the resulting field emission behavior were confirmed by Liu *et al.* [11] for SWNTs and Hata *et al.* for MWNTs [12].

10.4.1 Clean SWNT Field Emission Microscope Images

Field emission microscopy has been used to study metal surfaces for many decades [7]. For clean metal and semiconductor surfaces, the field-emitted electron beam produces a spatial distribution or "pattern" on the phosphor screen, which reflects the crystal symmetry of the emitting surface. Contrast arises in the image as a result of differences between the electron work functions of the crystal planes bisected by the surface and the differences between atomic steps in the crystal planes. Consequently, the detailed structure in the field emission pattern is representative of the electronic structure of the emitting surface.

Carbon nanotubes do not have a plane crystal structure as metals do; their electronic structure is very different. SWNTs are most often terminated with cap structures, and theorists have predicted that local states exist on the nanotube caps. Tamura and Tsukada computed that the several pentagon rings of carbon atoms on the cap enhance tunneling at each these locations [13]. The existence of these end states has been verified by Carroll *et al.* using scanning tunneling spectroscopy [14]. Thus, one would expect the field emission microscopy images of nanotubes to produce patterns corresponding to the spatial distribution of these local cap states.

There are numerous potential SWNT electronic structures. The typical nanotube cap illustrated in the literature is the fivefold-symmetry cap of the (10,0) tube with a C_{60}-type structure. However, Astakhova *et al.* identified seven caps that could theoretically exist at the end of this nanotube. While each cap contained six pentagons, most structures showed either two- or fourfold symmetry [15]. Thus, an FEM image, which is a map of the nanotube caps, can be much more complicated. Furthermore, Osawa *et al.* predict thousands of different cap configurations for the 90 SWNT structures with diameters smaller than 1.6 nm [16]. Thus, if a nanotube FEM image is a map of local electronic structure, and perhaps of the pentagonal carbon rings, one would expect to encounter a wide variety of patterns in a given population of nanotube structures. Further variety is expected because, for chiral nanotubes, the axis of symmetry of many nanotube caps does not lie along the axis of symmetry of the nanotube. This means that the side of the nanotube cap sits at the very end of the nanotube where the applied electric field is largest during field emission. As a result, the FEM image will be most intense off the axis of symmetry, producing a lopsided projection of the cap.

Dean *et al.* first reported experimentally obtained clean field emission microscope images showing more complicated structures anticipated from SWNT caps (Figure 10.1) [10, 17, 18]. They reported a clean nanotube image that was stable over time at room temperature for minutes to hours, until readsorption of an adsorbate. However, the same clean image was obtained again after thermally removing the adsorbate, over several months. Thus, they reported that the clean images were

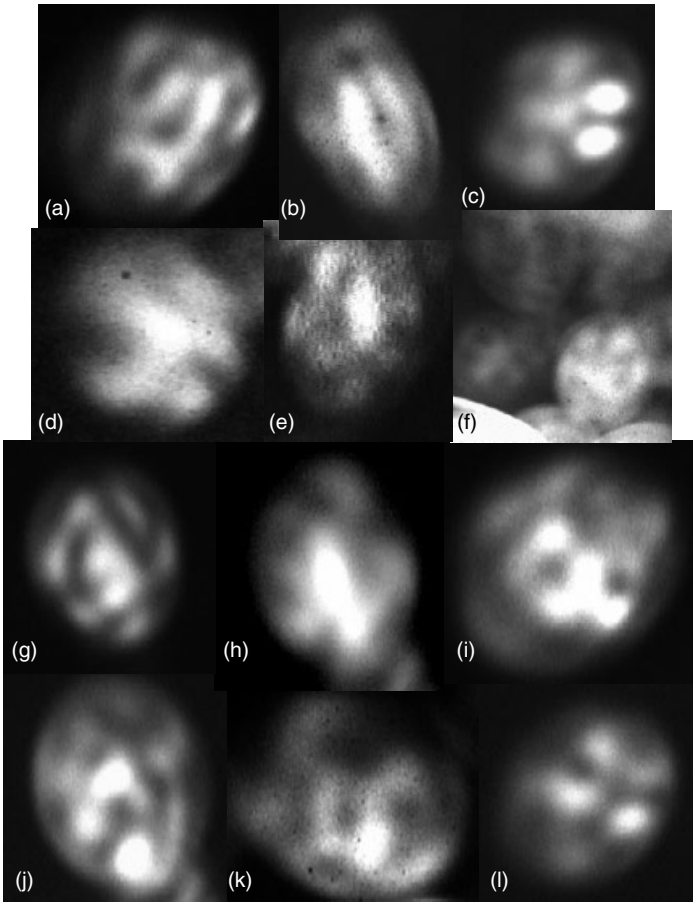

Figure 10.1 Examples of detailed structure within the FEM images of single-wall nanotubes. In (f), a group of closely spaced SWNTs all show fine structure. Images (g), (h), and (j) were obtained from Rice SWNTs. The rest of the images were obtained from Material and Electrochemical Research's arc-grown SWNTs.

repeatable, stable, and consistent with a clean nanotube surface. A fine-structure image with stable behavior was also reported by Sun *et al*. [19].

Dean *et al*. reported a multitude of different patterns, consistent with the large distribution of nanotube cap configurations occurring naturally. Some SWNT images show five- and sixfold symmetry, which they compared to scanning tunneling microscopy images of C_{60} molecules. These symmetries are expected for commonly proposed nanotube cap configurations of achiral nanotubes. More commonly, however, they reported that the clean nanotube images showed less symmetry, suggesting that other cap structures (especially chiral ones) were not as symmetrical [17].

Several authors have performed theoretical computations of the electronic structure of nanotube caps during field emission. They have created spatial maps of the local density of states in their efforts to explain the observed images [20, 21]. This work appears promising, but there is still an opportunity for additional understanding and measurement in this space.

Dean and Chalamala reported evidence for capped SWNTs, with all images having a clear structure in the middle (using several nanotube samples with narrow population distributions between 0.8 and 1.4 nm). They reported never observing an annular ring at room temperature. Even immediately following field evaporation (Section 10.1), they reported no evidence of open or uncapped nanotubes. However, Lui *et al.* [11] reported an annular SWNT field emission pattern with discrete dots in the ring from a SWNT bundle. They interpreted the image as an open (16, 0) nanotube. Consequently, more work is needed in this area to reach a general understanding.

An important question in interpreting these SWNT field emission microscope images is whether the FEM instrument is capable of resolving features with atomic resolution or nearly atomic resolution. Traditional field emission microscopy work on metals was performed on metal tips with large radii of curvature, thus limiting the resolution of the FEM to well short of atomic resolution. However, calculations by Ashworth show that with a tip radius of 5 Å, a resolution of 2 Å is possible [22], and Rose calculates that objects ~3 Å apart can be resolved with the FEM [23]. Binh *et al.* have resolved atomic scale images with the FEM [24]. In addition, Brodie presents strong evidence that extremely sharp objects and, particularly, whiskers with very high aspect ratios can and do show atomic resolution [25]. Finally, Dou *et al.* reported atomic resolution from sharpened W tips [26]. Both theoretical computations and a growing body of experimental work support atomic or near-atomic resolution for extremely sharp objects like nanotubes.

10.4.2 Clean SWNT *I–V*s

Current–voltage ($I-V$) measurements of clean SWNTs show stable, repeatable tunneling behavior and enormous obtainable current density. Dean *et al.* reported measurements for several samples, each containing a single emitting SWNT [27]. At 300 K, each clean nanotube surface produced a stable, reproducible $I-V$ curve, providing an excellent fit to the Fowler–Nordheim equation up to an emitted current ranging from 0.3 to 1 μA depending on the sample (Figure 10.2). The field emission image was also stable and reproducible.

The high overall current infers a high-current density exceeding 10^8 A cm^{-2} DC, using the mean diameter of the Rice University source nanotubes to estimate the area. This field emission current density is likely to be two orders of magnitude larger than can be obtained from typical metal field emitters without pulsing the bias voltage. A similarly high nanotube current density was measured under

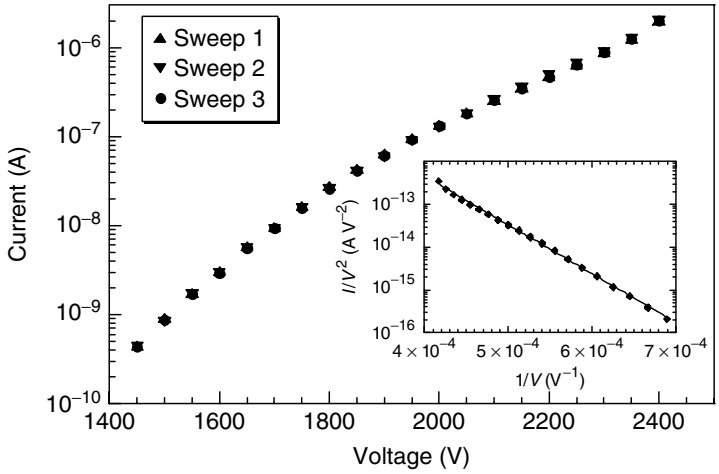

Figure 10.2 The current–voltage characteristic of a single, clean SWNT. The data fits the Fowler–Nordheim theory well (inset). The three symbols denote three consecutive I–V sweeps. (Reprinted with permission, Dean and Chalamala, *Appl. Phys. Lett.* (2002), American Institute of Physics [27].)

transport (non-field-emission conditions) on an individual SWNT by Yao and Dekker [28].

Dean *et al.* reported additional reproducible I–V behavior at electric fields up to 5% higher than discussed above, but the I–V curve in this region increased much faster than predicted by the Fowler–Nordheim equation, with maximum current limit reaching 2 μA. The field emission image also became blurred and a ring formed around the field emission image (Figure 10.3) [18, 29]. Ring formation has been observed by others in diode-type field emission configurations [30].

The increased-current blurred images and encircling ring suggest a local increase in temperature at the nanotube tip, resulting in thermally assisted field emission, and similar observations have been made for metals at high-current densities [31, 32]. In addition, nanometer-sized metal protrusions exhibit a local temperature increase exceeding 200 °C with only 4 nA of field emission current, as measured in the energy distribution of emitted electrons [33]. The metal protrusions were destroyed by melting at currents larger than 100 nA.

Dean *et al.* estimate that the local tip temperature reaches 1600 K based on the change in the nanotube's high current limit versus temperature [29]. Purcell *et al.* measured a similar increase in MWNT tip temperature at high current (from the slope of the electron energy distribution curves), demonstrating a temperature of 2000 K for a current of 1.3 μA [34]. Nanotubes can apparently handle an enormous current density without damage. However, currents exceeding the 1–2 μA range have been shown to cause permanent changes in the nanotubes, which is discussed in Section 10.4.4.

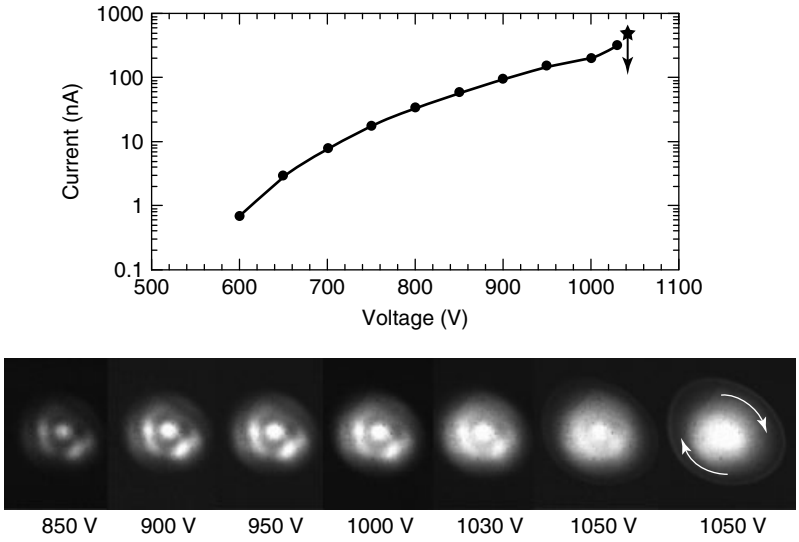

Figure 10.3 An I–V curve and corresponding field emission microscope images of a single SWNT. At extremely high currents, the slope of the ln (I)–V behavior begins to increase, the field emission image blurs, a ring forms around the image, and the image begins to rotate. (Reprinted with permission, Dean *et al*., *Appl. Phys. Lett.* (2001), American Institute of Physics [29].)

10.4.3 Thermal Field Emission

The previous section presented results concluding that nanotubes tips heat up at high currents producing thermally assisted field emission behavior without applied external heat. Thermal field emission behavior can also be examined by measuring both the change in current with temperature and the energy distribution of emitted electrons.

Of particular interest is that typical nanotube samples contain a mix of chiral (semiconducting) and nonchiral (metallic) nanotubes, with approximately 2 : 1 ratio. Dean *et al*. reported a significant difference in the temperature dependence of current from among nanotubes [35]. In a sample set containing 12 nanotubes, 4 increased in current by ~2 times between 300 and 1450 K (expected for metals with ~5 eV work function), while 8 increased by orders of magnitude (Figure 10.4a). The nanotubes with the highest current density at 1450 K were undetectable at 300 K under the applied voltage. The ratio of low thermally dependent nanotubes to high thermally dependent nanotubes in that experiment is the same as the anticipated ratio of conducting to semiconducting nanotubes, suggesting an explanation. Additional thermal field emission measurements also suggest a strong influence of the nanotube cap structure on the thermal dependence [17].

The energy distribution of field-emitted electrons provides some additional information. Dean *et al*. reported electron energy distribution measurements for

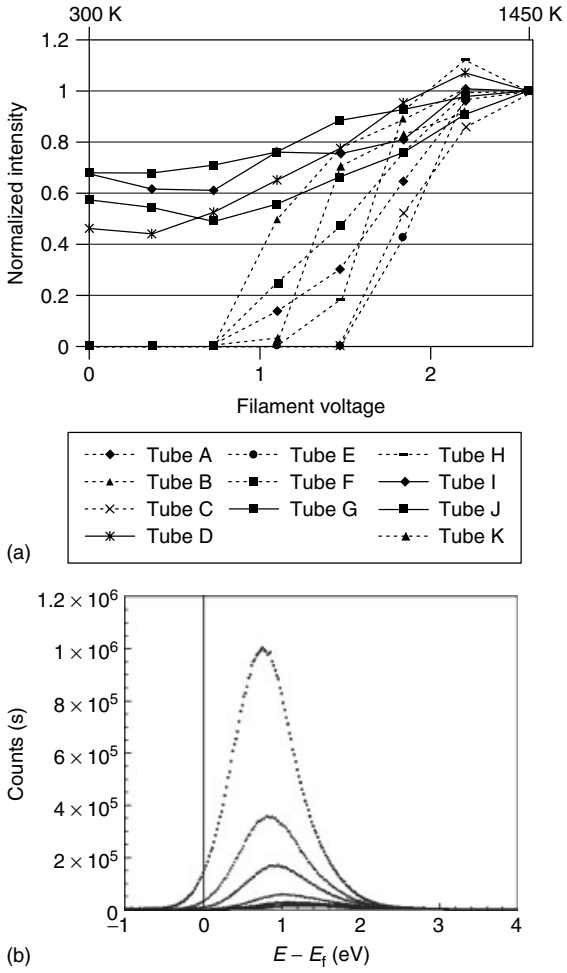

Figure 10.4 Current versus temperature behavior of 12 nanotubes mounted on a heater filament (a). Four of 12 nanotubes show metal-like temperature dependence, while the rest are highly temperature dependent. The current was computed from the measured integrated intensity of light on the phosphor screen. (Reprinted with permission, Dean *et al*., New Diamond and Frontier Carbon Technology (2002), MYU-KK [35].) (b) Electron energy distribution spectra of field-emitted electrons from SWNTs at 930 K showing the emission state well above the Fermi level. (Reprinted with permission, Dean *et al*., *Appl. Phys. Lett*. (1999), American Institute of Physics [36].)

a nanotube sample showing strong temperature dependence in the clean state. They report observing electron tunneling from broad states 1–2.8 eV above the Fermi level between 930 and 1160 K (Figure 10.4b) [36]. While it is unclear whether the multiple states were made from one or from a few nanotubes, the field emission behavior was clearly nonmetallic, and there was negligible current

density coming from the Fermi level region. The total emitted current at 930 K (emission from a single, broad peak, suggesting one CNT) was 120 nA, so the electric field was presumably large. The peak positions shifted linearly with applied voltage, characteristic of resonant tunneling states, rather than linearly with current, suggesting a conductivity limitation. These measurements suggest that cap states are primarily responsible for the temperature dependence of field emission from nanotubes showing a strong temperature dependency.

Collazo *et al.* reported measuring the electron energy distribution from a population of clean nanotubes [37]. Room temperature electron emission peaked at energies just below the Fermi level. Dean *et al.* also observed peaks only near the Fermi level at room temperature. Collazo *et al.* did not report measurements at elevated temperature.

10.4.4
High Current and Field Evaporation

Section 10.4.3 discussed the stable and reproducible field emission from clean SWNTs, although at high currents researchers found that nanotubes were getting hot. Dean *et al.* reported that above a threshold current of 1–2 μA per SWNT, the individual nanotubes irreversibly changed [29]. Movement commenced within the blurred center of the field emission image. They observed that the motion was an infrequent ''pop'' for currents just above the threshold, but the speed of motion increased rapidly with increasing current. At currents two to three times above the threshold, the movement was so frequent that it appeared as the continuous spinning of a blurred image with the frequency of rotation exceeding 5 Hz. The intensity of the outer ring also fluctuated as the blurred central image spun (Figure 10.5).

Reducing the current below the threshold stopped the motion, apparently freezing the field emission image in place. The field emission image was generally not the same as the original. The new field emission image and associated $I-V$ characteristics were stable and reversible under all conditions below the threshold current. In short, movement in the field emission images at high current coincided

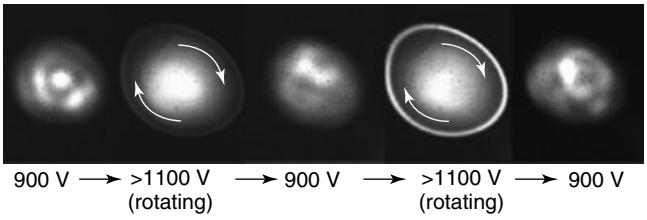

Figure 10.5 The field emission image of an SWNT showing the blurring at high currents. A ring forms around the image and the nodes in the central image spin rapidly. When the current is reduced, a different field emission image is produced, indicating that the cap structure has changed. (Reprinted with permission, Dean *et al.*, *Appl. Phys. Lett.* (2001), American Institute of Physics [29].)

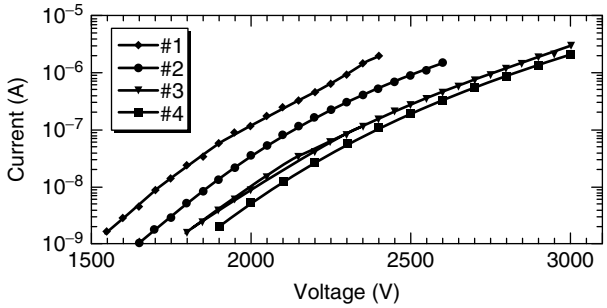

Figure 10.6 The *I–V* behavior of an individual SWNT degrading during periods of emission at high currents, accompanied by rapid movement in the FEM image. Ten minutes of high-current emission separate curves 1 and 4. (Reprinted with permission, Dean *et al*., *Appl. Phys. Lett*. (2001), American Institute of Physics [29].)

with a permanent change in the spatial distribution of field emission current from SWNTs (Figure 10.5).

For small periods of movement in the FEM image, the current–voltage behavior showed only minor changes (as will be discussed later). Allowing the spinning motion to proceed for several minutes under continuous bias conditions resulted in a new FEM image with degraded *I–V* characteristics. The shift in the *I–V* curve is consistent with a reduction in the field enhancement of the nanotube by shortening as much as 25% (Figure 10.6).

Dean *et al*. explained the observed phenomenon as thermally assisted field evaporation [29]. Traditional field evaporation is measured under the opposite bias conditions of field emission, and requires substantially higher electric fields. Hata *et al*. experimentally measured room temperature field evaporation of ionized carbon clusters from both MWNTs and SWNTs at an electric field of $\sim$10 V nm^{-1} under the opposite bias conditions (field ion microscopy) used for field emission [38]. The increase in temperature of the nanotube at high current lowers the evaporation barrier, allowing field evaporation under electric fields compatible with field emission, and with the same polarity. Interestingly, thermally assisted field evaporation of metals under field emission conditions catastrophically destroyed emitters in great arcs. In contrast, SWNT thermal field evaporation appeared to be gentle, and generally stable.

Dean *et al*. reported no evidence for open-ended SWNT FEM images similar to the images Saito *et al*. observed for MWNTs [39]. The new FEM patterns that appeared when the voltage was reduced were consistent with an immediate reformation of a new end structure.

These reported changes in field emission images upon thermal evaporation opened up the possibility of measuring the variety of cap structures that could occur on just one SWNT. Investigators had proposed that there were a finite number of atomic structures that an SWNT would support. If the electronic

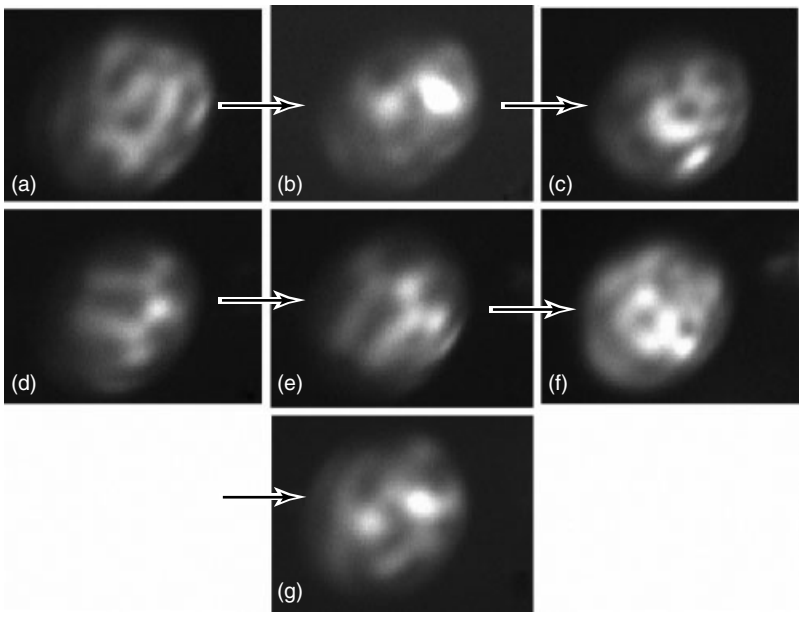

Figure 10.7 A subset of field emission images obtained from a single nanotube showing repeating patterns. Patterns (b) and (g) are identical, (d) and (e) are rotated, and (c) and (f) are closely related. Patterns presented are in the order they were obtained, but several intermediate patterns have not been included. (Reprinted with permission, Dean *et al.*, *J. Vac. Sci. Technol.* (2002), American Institute of Physics [17].)

structure and the atomic structures were closely linked, there might be only a finite number of nanotube patterns available. By repeatedly field-evaporating the end of a nanotube, Dean *et al.* reported that some nanotubes produced more than 50 unique patterns without any pattern repetition, while others showed repetition of exact or very similar patterns (Figure 10.7) [17].

10.4.5 Anomalous High-Temperature Behavior

Dean *et al.* repeatedly observed instability in SWNT field emission which has not been adequately explained [18]. Field emission current was reported to be stable for clean SWNTs at room temperature. This current was also stable for temperatures above 900 K, but only for higher currents (and voltages/electric fields). Below a threshold voltage, which was a found to be a linearly increasing function of temperature, the emission current dropped rapidly over time, typically decreasing by two orders of magnitude over 100 s. The entire $I-V$ curve was then shifted to higher voltages and continued to shift over time during field emission. However, application of a voltage much higher than the degradation threshold caused an increase in current over time (at that fixed voltage) which accelerated rapidly over nominally 20 s. This current increase terminated abruptly when the original current

(at that voltage) was reached, restoring completely the original $I-V$ curve. Again, this behavior was found to be extremely reproducible on each sample, among samples, and among nanotubes from different sources and production techniques; yet, no mechanism for this behavior has yet been proposed.

10.5 SWNT-Adsorbate Field Emission

Unless the field-emitting surfaces of nanotubes are specifically cleaned, field emission behavior of nanotubes is dominated by adsorbate–nanotube electronic states. These states produce distinctive field emission patterns, current fluctuations, and temperature behaviors, which are described in the following section.

10.5.1 Field Emission Microscopy

Early SWNT field emission experiments reported lobed field emission images on phosphor-coated anodes [40, 41]. In fact, these images have been commonly observed by researchers using electrode geometries that provide magnification [30, 42, 43]. Dean and Chalamala proposed that these images resulted from chemisorbed adsorbates states [10]. First, they documented that SWNTs showed field emission patterns with one, two, and four lobes (Figure 10.8). However, a large percentage of these lobes (>50%) appeared to be lopsided versions of the three basic patterns, which would occur if the axis of symmetry of the field-emitting surface was not along the axis of symmetry of the nanotube. This structure typically occurs in chiral nanotubes, where the apex is not along the axis of symmetry of the nanotube. Most of the time, the images were not constant with time; they flickered and changed patterns.

In the literature, lobe-type field emission images were readily observed on metal surfaces, and were found to originate from preferential tunneling through specific adsorbate molecules [7, 44–46]. For example, the emission patterns of large chemisorbed molecules on metals produce bright one-, two-, and four-lobed images superimposed over the metal images. These surface states create a resonant tunneling condition for electrons, greatly increasing the local tunneling current at the molecule [47, 48]. While the mechanism is tunneling, and often produces a good linear fit on a $\ln(I/V^2)$ versus $1/V$ plot, it is not described by the Fowler–Nordheim model, and the slope is not proportional to $\phi^{3/2}$ (where ϕ is the emitter work function) [45].

The behavior of adsorbates on metal surfaces had been studied extensively, and several other behaviors had been identified from field emission images: (i) the image nodes changed with time, (ii) the rate of change of the image increased with temperature, (iii) the images were removed by desorbing the molecule, leaving the image of a clean metal surface, (iv) the adsorbates readsorbed onto a clean nanotube surface by supplying adsorbate molecules, and (v) the adsorbate substantially increases the local field emission current. Dean and Chalamala verified

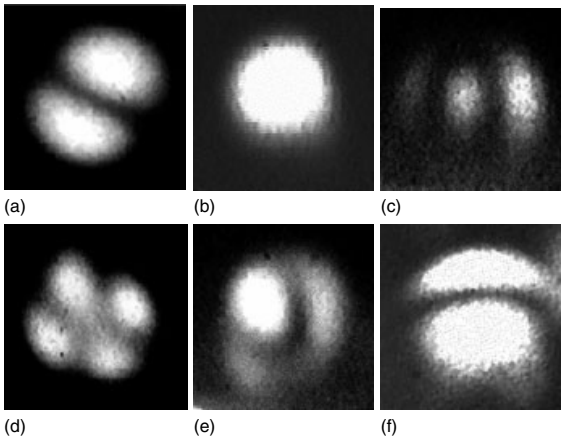

Figure 10.8 Field emission patterns with one to four lobes observed at room temperature (a–d). Tilted versions of the symmetrical lobed patterns that probably occur when electrons are emitted from surfaces not parallel to the anode (e–f). (Reprinted with permission, Dean *et al*., *J. Appl. Phys.* (1999), American Institute of Physics [10].)

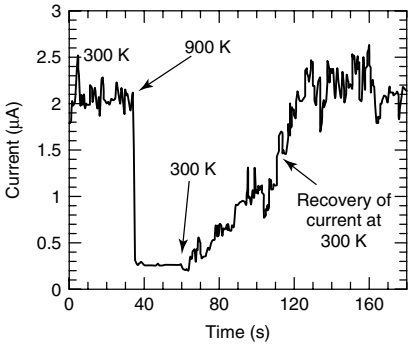

Figure 10.9 Current versus time showing a drop in current as the temperature is raised to 900 K, and a recovery of current when the temperature is returned to 300 K. (Reprinted with permission, Dean *et al*., *J. Vac. Sci. Technol*. (1999), American Institute of Physics [18].)

all of these behaviors in the SWNT FEM images (Figure 10.9) [10]. In addition, they reported that adsorbates on SWNTs increased the total tunneling current by up to two orders of magnitude, an observation verified by Collazo *et al*. [37].

Several groups have sought the identity of the adsorbate species responsible for enhanced SWNT emission. Collazo *et al*., Dean *et al*., and Nilsson *et al*. each reported that in a baked out vacuum system under UHV conditions, the time to reabsorb adsorbates on a clean surface and recover the full current was approximately 1 h [18, 37, 42]. However, Dean *et al*. observed that, if the phosphor was omitted

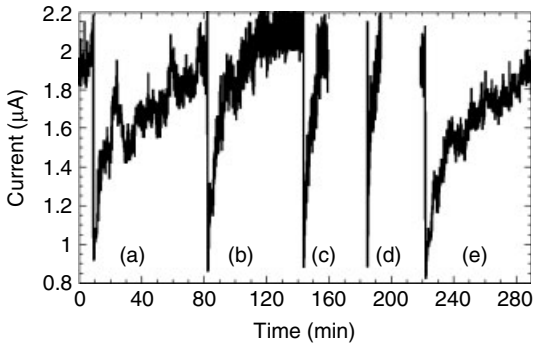

Figure 10.10 The effect of water partial pressure on the recovery time of field emission current after heating the emitter to 900 K. (a) 5×10^{-9} Torr H_2O, (b) 5×10^{-8} Torr H_2O, (c) 4×10^{-7} Torr H_2O, (d) 5×10^{-6} Torr H_2O, and (e) 2×10^{-9} Torr H_2O after 3 h of pumping after measurement of (d). (Reprinted with permission, Dean *et al.*, *J. Vac. Sci. Technol.* (1999), American Institute of Physics [18].)

from the bakeout, the recovery time was only 3 min, suggesting that the adsorbate responsible was present in the phosphor and could be outgassed below 60 °C. Nilsson *et al.* verified this observation, also reporting that the adsorbate was present in the phosphor. Dean *et al.* performed gas introduction experiments in a field emission microscope with H_2, O_2, H_2O, and Ar. The effects of CO and CO_2 were also screened. They reported that addition of a partial pressure of water produced a strong response on the current recovery time (<60 s), whereas the other gases showed no effect (Figure 10.10). Consequently, Dean *et al.* concluded that water or a related species (OH^- or H_3O^+) was responsible for the adsorbate states. However, Nilsson *et al.* reported no change in emission with the introduction of H_2 or water. Consequently, additional investigation is needed in this area.

Finally, it should be noted that very similar adsorbate field emission patterns have been reported from field-emitting MWNTs, diamond-like carbon, nanodiamond, microcrystalline graphite, and nanocrystalline graphite [12, 35]. (In the case of MWNTs, the surface is large enough to accommodate multiple, spatially isolated adsorbates.) Clearly, this chemical interaction is a property of carbon materials in general.

10.5.2 Electron Energy Distributions

The mechanisms proposed for adsorbate-state tunneling incorporate a resonant electronic state. These models predict that the energy distribution of emitted electrons will show a sharp peak at the energy level of the resonant state. Both Dean *et al.* and Collazo *et al.* reported electron energy distribution measurements of SWNTs emitting from adsorbate states in which the energy peak is located just below the Fermi level [36, 37]. Collazo *et al.* measured a clear difference between the peak of the clean nanotubes and the peak of adsorbate states on nanotubes. The

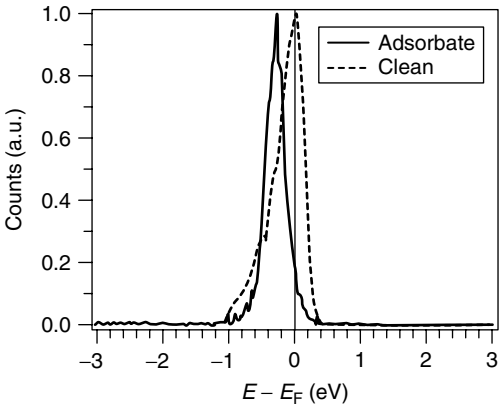

Figure 10.11 Field emission electron energy distribution spectra of nanotubes at an applied bias of 757 V for the clean and adsorbate state. (Reprinted with permission, Collazo *et al*., *Diamond Relat. Mater.* (2002), Elsevier [37].)

clean nanotube energy distribution peak was located at the Fermi level and showed a typical asymmetric peak shape characteristic of metallic emitters. In contrast, the adsorbate peak was shifted approximately 0.4 eV below the Fermi level and had a symmetrical shape (Figure 10.11). The adsorbate peak position was less dependent on voltage than the Fermi level peak. Collazo *et al.* concludes that the adsorbates emit through a resonant state located close to the Fermi level.

10.5.3
Current Saturation and Field-Emission-Induced Surface Cleaning

Several investigators, including Collins and Zettl [49, 50], Bonard *et al*. [51], and Xu and Brandes [52], have shown that both SWNTs and MWNTs exhibit field emission current saturation at high fields. This property is of particular interest for field emission displays (FEDs) because existing prototypes require external current-limiting resistors in series with each emitter. These resistors are necessary with refractory metal and silicon emitters because they eliminate current runaway and arcing and improve current uniformity among emitters [53]. The intrinsic emission current saturation characteristics of carbon nanotubes may make them a better emitter choice for display applications.

The emission current saturation reported in the above references was observed in measurements of ensembles of emitting nanotubes; so, it was unclear whether saturation was an ensemble behavior or an individual SWNT behavior. However, current saturation had been observed in all test geometries including parallel plate, ball-plane, and point-plane (FEM). It had also been reported under vacuum conditions ranging from 10^{-5} to 10^{-9} Torr.

Using several different samples, each with a single, isolated SWNT emitter, investigators reported that current saturation was a property of a single SWNT

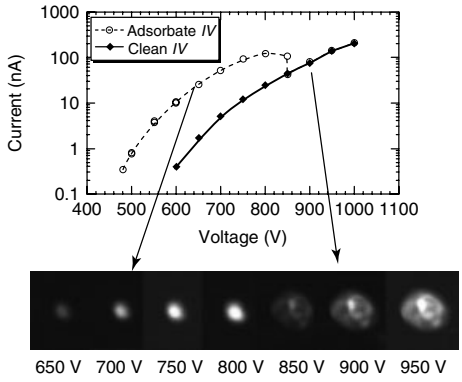

(a)

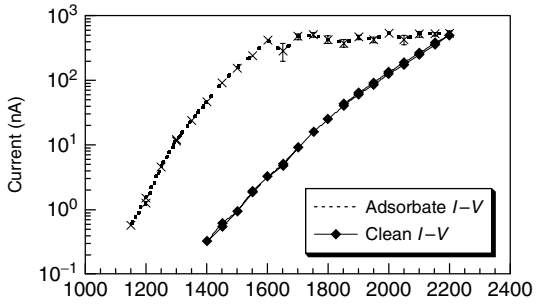

(b)

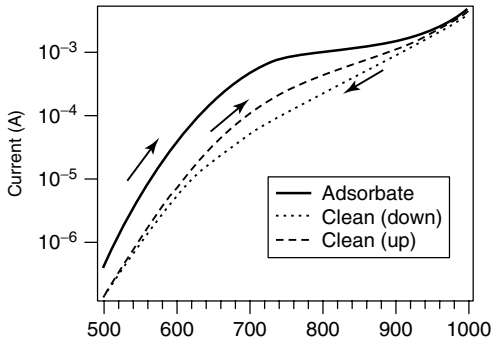

(c)

Figure 10.12 The field emission current of an individual SWNT saturating at approximately 100 nA because the adsorbate molecule desorbs. The *I*–*V* curve follows the dashed line until desorption, whence it follows the solid line for all voltages (a). In a typical case, the desorption event occurs through multiple states leading to a broad, saturated region (b). In (b) the error bars represent the standard deviation of current fluctuation during the current measurement at each point. (Reprinted with permission, Dean *et al*., New Diamond and Frontier Carbon Technology (2002), MYU-KK [35].) (c) Current–voltage (*I*–*V*) curve for the SWNT thin film. (Reprinted with permission from Collazo *et al*., *Diamond Relat. Mater.* (2002), Elsevier [37].)

[27, 35]. They found that a clean nanotube emitter under UHV conditions showed Fowler–Nordheim tunneling behavior with no saturation whatsoever, while the same nanotube under nonideal vacuum conditions demonstrated strong $I–V$ current saturation. The low-current data increased approximately exponentially with voltage over >50% increase in electric field, as expected. However, above approximately 100–300 nA per nanotube (varying by sample), the current increased only minimally over the next 30% increase in field.

After considering a host of possible mechanisms, Dean *et al.* concluded that, as the current increased, the end of the nanotube heated up, causing the adsorbate to occupy less favorable tunneling states until it finally desorbed. The result was an $I–V$ curve that looked saturated (Figure 10.12a and b). As part of their description, they reported that, as the current increased, both the motion of the adsorbate in the FEM image and the current fluctuation at constant extraction voltage increased substantially, peaking at about 100 nA [35]. With the application of sufficient electric field in the saturated current region, the adsorbate was eventually removed, and the $I–V$ curve transitioned into the clean-emitter $I–V$ behavior. Moreover, the FEM image motion, current fluctuation behavior, and desorption event could all be achieved at constant current simply by applying heat from an external source.

This self-cleaning behavior led to an $I–V$ hysteresis under proper UHV conditions with a high-current ''adsorbate-state'' upsweep and a low-current ''clean-nanotube'' downsweep. Collazo *et al.* went further to demonstrate this result with a film of SWNTs containing a great number of emitting nanotubes under UHV conditions (Figure 10.12c) [37].

However, under poor vacuum (10^{-7} Torr, unbaked chamber) Dean *et al.* reported that readsorption of adsorbates was so rapid that the downsweep tracked back along the adsorbate-state upsweep curve, even for single SWNTs. No hysteresis but just a repeatable saturated $I–V$ curve was observed.

Cleaner conditions than those above, which are required to eliminate the adsorbates, are not met in most nanotube investigations reported in the literature. Moreover, it is not clear whether sufficient cleanliness conditions will be met in practical devices to eliminate adsorbates. Consequently, field emission from adsorbates is an important aspect of both nanotube characterization and nanotube-based devices.

10.6
Field Emission Stability

Recent research on carbon-based field emitters has focused on properties necessary for FEDs and other vacuum microelectronic applications. These devices require thousands of hours of highly stable emitter operation.

The first FEDs employed metal-tip field emitters. Metal field emission tips are modified by oxidation and sputtering during operation. They have a tendency to sharpen over time, providing a positive feedback loop which results in their

destruction by a catastrophic arc, often in less than 1 h under UHV conditions [54–56]. To reduce or eliminate device failures due to arcing, many vacuum microelectronic devices employ a series resistance in the emitter circuit to provide negative feedback, thus creating stability.

Surprisingly, SWNTs do not need a ballast resistor in series to prevent current runaway. Stable operation has been demonstrated for hundreds of hours under the same conditions that destroy metal emitters in an hour. It is believed that strong covalent bonding, resistance to sputtering and oxidation, adsorbate current saturation mechanisms, and a gentle field evaporation process all contribute to this stability.

10.6.1
Current Fluctuation

As shown in previous sections, a clean SWNT surface is very stable over time. For applications that support a UHV environment, and tolerate periodic surface cleans of $>600\,^{\circ}C$ (for example, scanning electron microscope electron sources), this stability can be realized. For most other applications, adsorbate molecules populate the surface. Current from a field emitter is very sensitive to the presence of adsorbate molecules. More importantly, adsorbate molecules occasionally move, resulting in large current swings. Current fluctuation (or noise) is a major reason why metal microtip field emission sources were not able to displace solid-state semiconductors in amplifier applications. SWNT adsorbate-state field emission increases SWNT emission current by 10–100 times, meaning that SWNTs are particularly noisy.

Dean *et al*. reported that SWNT fluctuation was a function of nanotube temperature. Current fluctuation of an individual SWNT (with adsorbates) increased by roughly an order of magnitude between room temperature and approximately $225\,^{\circ}C$, which is the peak fluctuation temperature. More importantly, extracting field emission current from nanotubes heated them, thereby increasing their current fluctuation. They found that fluctuations peaked at approximately 100 nA of current per nanotube, which is a fairly typical operating condition (Figure 10.13).

Consequently, SWNTs are noisy field emission sources. Noise can be minimized by employing them in applications requiring great numbers of emitters in parallel, thereby averaging out the fluctuations. FEDs make the best use of nanotube averaging, often employing hundreds or thousands of nanotubes per pixel.

10.6.2
Current Degradation

SWNTs are reported to be more susceptible to degradation than other emitters. Bonard *et al*. reported that SWNT field emitters degraded faster than MWNT emitters [51]. Uemura *et al*. reported that DWNTs (the smallest of MWNTs) provided significantly enhanced stability over SWNTs, without sacrificing the sharp

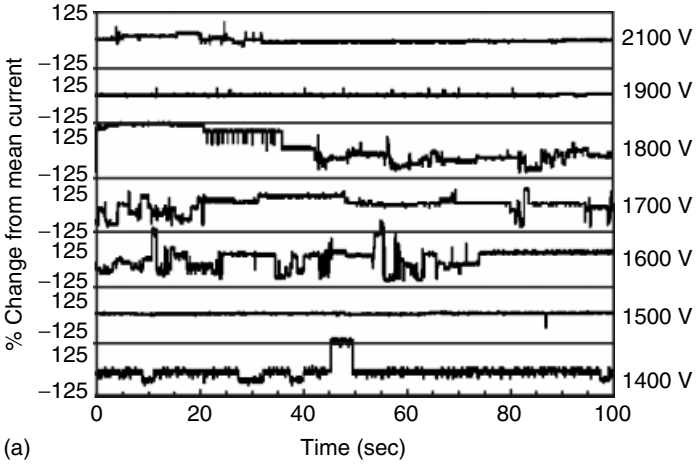
% Change from mean current
125
−125
2100 V
1900 V
1800 V
1700 V
1600 V
1500 V
1400 V
0
20
40
60
80
100
Time (sec)

(a)

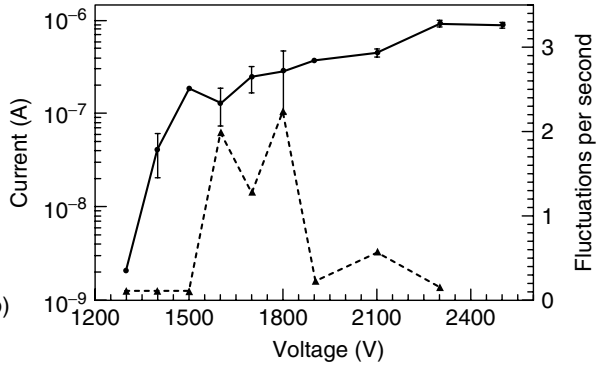
Current (A)
10^{-6}
10^{-7}
10^{-8}
10^{-9}
Fluctuations per second
3
2
1
0
1200
1500
1800
2100
2400
Voltage (V)

(b)

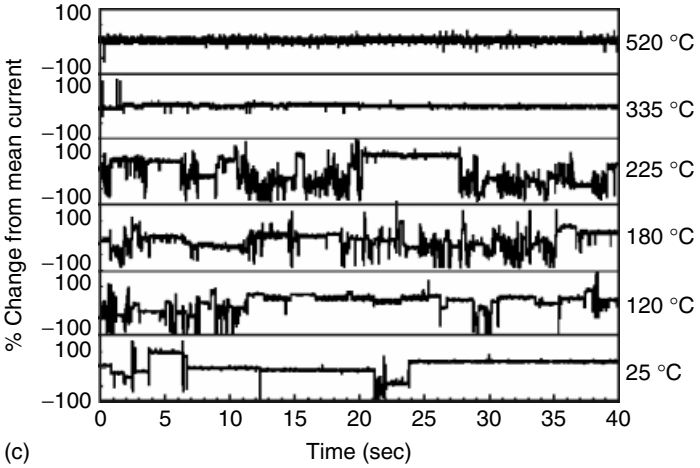
% Change from mean current
100
−100
520 °C
335 °C
225 °C
180 °C
120 °C
25 °C
0
5
10
15
20
25
30
35
40
Time (sec)

(c)

Figure 10.13 The fluctuation in current from an individual SWNT increasing with increasing current through the onset point of current saturation. In (a) and (b), the current saturation onset occurs at a nominal current of 100 nA, corresponding to an applied voltage of 1600 V. The magnitude and frequency of current fluctuation peak near the saturation onset, with a fluctuation rate 100 times that at lower voltages (b). Above the strongly current-saturated region (1600–1800 V), the current fluctuation decreases with increasing current. Errors bars in (b) depict the standard deviation of current magnitude measured at each point. In (c), external thermal excitation greatly increases the current fluctuation frequency, producing a fluctuation behavior similar to that shown in (b), but without increasing the current. The current at room temperature is nominally 300 nA, but it decreases with increasing temperature to 200 nA at 225 °C and 60 nA at 520 °C as adsorbates are removed. The maximum current fluctuation rate occurs at excitation conditions of 225 °C and 200 nA. (Reprinted with permission, Dean *et al*., *New Diamond Front. Carbon Technol*. (2002), MYU-KK [35].)

geometry [57]. To find out what factors contribute to SWNT degradation, Dean and Chalamala demonstrated 350 h of direct current (100% duty cycle) operation without degradation in UHV field emission microscope experiments [58]. They also reported no degradation when exposed to substantial H_2 and Ar partial pressures, but substantial degradation with 10^{-8} Torr of O_2 present. A small amount of degradation was also observed with 10^{-6} Torr of water present (Figure 10.14).

Dean and Chalamala proposed a reactive sputter-etching mechanism to explain their data, noting that studies on the sputter-etching of graphite show much faster etching in O_2 than in Ar, demonstrating a reactive ion etching effect [59]. In addition, carbon etching studies have also found that water chemically enhances the sputter-etching of carbon [59]. Nilsson verified that H_2 partial pressures had

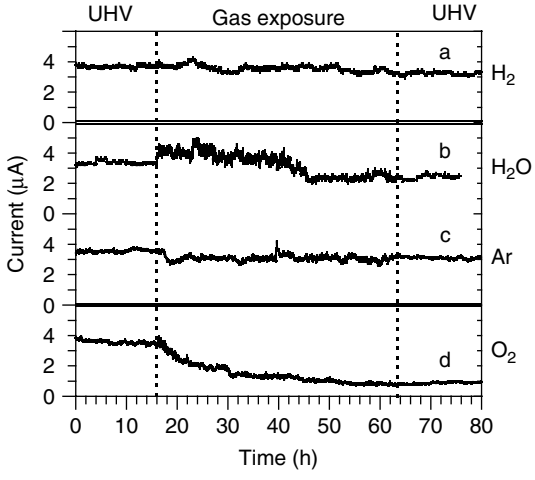

Figure 10.14 Emitter operation under various gas ambients: (a) 0.15 Torr s H_2 (150 000 Langmuir), (b–d) 0.015 Torr s (15 000 Langmuir). (Reprinted with permission, Dean *et al*., *Appl. Phys. Lett*. (1999), American Institute of Physics [58].)

negligible effect, but O_2 partial pressures degraded emission [42]. Thus, reactive sputter-etching explains the irreversible current decrease observed with both O_2 and H_2O, although O_2 exposure is considerably more severe.

10.7 Conclusions

Clean SWNTs are highly stable and reproducible field emitters under UHV conditions. Scientists have observed structure in field emission microscope images indicative of the local electronic structure of nanotube caps. In addition, electron energy distribution measurements and thermal field emission behavior also suggest that nanotubes emit through special cap electronic states.

However, adsorbate molecules strongly and readily modify SWNT field emission behavior. It is not clear whether sufficient cleanliness conditions will be met in practical devices to eliminate adsorbates. Consequently, field emission from adsorbates is an important (and perhaps dominant) aspect of both nanotube characterization and nanotube-based devices. While enhancing overall current, these adsorbates create current noise, which is objectionable for many applications. Thus, SWNT field emitters are most suited to device designs that support periodic cleaning, or incorporate hundreds of electrically parallel emitters to average out current fluctuations.

On the positive side, SWNTs show incredible stability when compared to metals. They can source orders of magnitude more current density without degradation; they are effectively immune from electromigration; and they degrade gently under high-current, high-temperature, and high-electric-field conditions. Moreover, their physics provides for current self-limiting mechanisms, rather than runaway feedback mechanisms in metals. However, SWNT field emitters are degraded by oxygen in the environment. MWNTs, even very small diameter ones, are more robust to oxygen. It is hoped that this understanding of SWNT field emitters, including both their strengths and their weaknesses, will lead to new and exciting FEDs.

References

1. Fowler, R.H. and Nordheim, L. (1928) *Proc. R. Soc. London*, **A119**, 173.
2. Modinos, A. (1984) *Field, Thermionic, and Secondary Electron Emission Spectroscopy*, Plenum, New York.
3. For example: Rinzler, A.G., Liu, J., Dai, H., Nikolaev, P., Huffman, C.B., Rodriguez-Macias, F.J., Boul, P.J., Lu, A.H., Heymann, D., Colbert, D.T., Lee, R.S., Fischer, J.E., Rao, A.M., Eklund, P.C., and Smalley, R.E. (1998) *Appl. Phys. A*, **67**, 29.
4. Saito, R., Fujita, M., Dresselhaus, G., and Dresselhaus, M.S. (1992) *Appl. Phys. Lett.*, **60**, 2204.
5. Zhu, W., Kochanski, G.P., Jin, S., and Seibles, L. (1996) *J. Vac. Sci. Technol., B*, **14**, 2011.
6. Coll, B.F., Jaskie, J.E., Markham, J.L., Menu, E.P., Talin, A.A., and vonAllmen, P. (1998) *Covalently Bonded Disordered*

Thin Films, MRS Symposium Proceedings, vol. 498 (eds M.P. Siegal, W.I., Milne, and J.E., Jaskie), Materials Research Society, Warrendale, p. 185.
7. Dyke, W.P. and Dolan, W.W. (1956) *Adv. Electron. Electron Phys.*, **8**, 89.
8. Arnold, M.S., Green, A.A., Hulvat, J.F., Stupp, S.I., and Hersam, M.C. (2006) *Nat. Nanotechnol.*, **1**, 61.
9. Gomer, R. (1993) *Field Emission and Field Ionization*, American Institute of Physics, New York, p. 34 and 148.
10. Dean, K.A. and Chalamala, B.R. (1999) Field emission microscopy of carbon nanotube caps. *J. Appl. Phys.*, **85**, 3832.
11. Liu, W., Hou, S., Zhang, Z., Zhang, G., Gu, Z., Luo, J., Zhao, X., and Xue, Z. (2003) Atomically resolved field emission patterns of single-walled carbon nanotubes. *Ultramicroscopy*, **94**, 175.
12. Hata, K., Takakura, A., and Saito, Y. (2001) Field emission microscopy of adsorption and desorption of residual gas molecules on a carbon nanotube tip. *Surf. Sci.*, **490**, 296.
13. Tamura, R. and Tsukada, M. (1995) *Phys. Rev. B*, **52**, 6015.
14. Carroll, D.L., Redlich, P., Ajayan, P.M., Charlier, J.C., Blasé, X., De Vita, A., and Car, R. (1997) *Phys. Rev. Lett.*, **78**, 2811.
15. Astakhova, T.Yu., Buzulukova, N.Yu., Vinogradov, G.A., and Osawa, E. (1999) *Fullerene Sci. Technol.*, **7**, 223.
16. Osawa, E., Yoshida, M., Ueno, H., Sage, S., and Yoshida, E. (1999) *Fullerene Sci. Technol.*, **7**, 239.
17. Dean, K.A. and Chalamala, B.R. (2003) Experimental studies of the cap structure of single-walled carbon nanotubes. *J. Vac. Sci. Technol., B*, **21**, 868.
18. Dean, K.A., von Allmen, P., and Chalamala, B.R. (1999) Three behavioral states observed in field emission from single-walled carbon nanotubes. *J. Vac. Sci. Technol., B*, **17**, 1959.
19. Sun, J.P., Zhang, Z.X., Hou, S.M., Zhang, G.M., Gu, Z.N., Zhao, X.Y., Liu, W.M., and Xue, Z.Q. (2002) *Appl. Phys. A*, **75**, 479–483.
20. Buldum, A. and Lu, J.P. (2003) *Phys. Rev. Lett.*, **91**, 236801.
21. Khazaei, M., Dean, K.A., Farajian, A., and Kawazoe, Y. (2007) *J. Phys. Chem. C*, **111**, 6690.
22. Ashworth, F. (1951) *Adv. Electron.*, **3**, 1.
23. Rose, D.J. (1956) *J. Appl. Phys.*, **27**, 215.
24. Binh, V.T., Garcia, N., and Purcell, S.T. (1996) in *Advances in Imaging and Electron Physics*, vol. 95 (ed. P. Hawkes), Academic, New York, pp. 63–153.
25. Brodie, I. (1978) *Surf. Sci.*, **70**, 186.
26. Dou, J., Chen, E., Zhu, C., and Yang, D. (2000) *J. Vac. Sci. Technol., B*, **18**, 2681.
27. Dean, K.A. and Chalamala, B.R. (2000) Current saturation mechanisms in carbon nanotube field emitters. *Appl. Phys. Lett.*, **76**, 375.
28. Yao, Z., Kane, C.L., and Dekker, C. (2000) *Phys. Rev. Lett.*, **84**, 2941.
29. Dean, K.A., Burgin, T.P., and Chalamala, B.R. (2001) Evaporation of carbon nanotubes during electron field emission. *Appl. Phys. Lett.*, **79**, 1873.
30. Zhu, W., Bower, C., Zhou, O., Kochanski, G.P., and Jin, S. (1999) *Appl. Phys. Lett.*, **75**, 873.
31. Latham, R.V. (ed.) (1995) *High Voltage Vacuum Insulation*, Academic Press, New York, pp. 211–218.
32. Dyke, W.P., Trolan, J.K., Martin, E.E., and Barbour, J.P. (1953) *Phys. Rev.*, **91**, 1043.
33. (a) Binh, V.T., Purcell, S.T., Gardet, G., and Garcia, N. (1992) *Surf. Sci. Lett.* **279**, 197; (b) Also done via TED in review article, Binh, V.T., Garcia, N., and Purcell, S.T. (1996) *Advances in Imaging and Electron Physics*, vol. 95 (ed. P. Hawkes), Academic Press, New York, pp. 63–153.
34. Purcell, S.T., Vincent, P., Journet, C., and Binh, V.T. (2002) *Phys. Rev. Lett.*, **88**, 105502.
35. Dean, K.A., Chalamala, B.R., Coll, B.F., Wei, Y., Xie, C.G., and Jaskie, J.E. (2002) *New Diamond Front. Carbon Technol.*, **12**, 165.
36. Dean, K.A., Groening, O., Kuttel, O.M., and Schlapbach, L. (1999) Nanotube electronic states observed with thermal field emission electron spectroscopy. *Appl. Phys. Lett.*, **75**, 2773.
37. Collazo, R., Schlesser, R., and Sitar, Z. (2002) *Diamond Relat. Mater.*, **11**, 769.
38. Hata, K., Ariff, M., Tohji, K., and Saito, Y. (1999) *Chem. Phys. Lett.*, **308**, 343.

39. Saito, Y., Hamaguchi, K., Hata, K., Unichida, K., Tasaka, Y., Ikazaki, F., Yumura, M., Kasuya, A., and Nishina, Y. (1997) *Nature*, **389**, 554.

40. de Heer, W.A., Chatelain, A., and Ugarte, D. (1995) *Science*, **270**, 1179.

41. Saito, Y., Hata, K., and Murata, T. (2000) *Jpn. J. Appl. Phys.*, **39** (Pt 2), 271.

42. Nilsson, L., Groening, O., Kuettel, O., Groening, P., and Schlapbach, L. (2002) *J. Vac. Sci. Technol., B*, **20**, 326.

43. Bonard, J.-M., Salvetat, J.-P., Stockli, T., de Heer, W.A., Forro, L., and Chatelain, A. (1998) *Appl. Phys. Lett.*, **73**, 918.

44. Melmed, A.J. and Muller, E.W. (1958) *J. Chem. Phys.*, **29**, 1037.

45. Morikawa, H., Okamoto, K., Yoshino, Y., Iwatsu, F., and Terao, T. (1997) *Jpn. J. Appl. Phys.*, **36**, 583.

46. Gomer, R. and Speer, D.A. (1953) Molecular images with the projection microscope. The ionization potential of zinc phthalocyanine. *J. Chem. Phys.*, **21**, 73.

47. Duke, C.B. and Alferieff, M.E. (1967) Field emission through atoms adsorbed on a metal surface. *J. Chem. Phys.*, **46**, 923.

48. Swanson, L.W. and Crouser, L.C. (1970) *Surf. Sci.*, **23**, 1.

49. Collins, P.G. and Zettl, A. (1997) *Phys. Rev. B*, **55**, 9391.

50. Collins, P.G. and Zettl, A. (1996) *Appl. Phys. Lett.*, **69**, 1969.

51. Bonard, J.-M., Maier, F., Stockli, T., Chatelain, A., de Heer, W.A., Salvetat, J.-P., and Forro, L. (1998) *Ultramicroscopy*, **73**, 918.

52. Xu, X. and Brandes, G.R. (1999) *Appl. Phys. Lett.*, **74**, 2549.

53. Ghis, A., Meyer, R., Rambaud, P., Levy, F., and Leroux, T. (1991) *IEEE Trans. Electron Devices*, **38**, 2320.

54. Janssen, A.P. and Jones, J.P. (1971) The sharpening of field emitter tips by ion sputtering. *J. Phys. D*, **4**, 118.

55. Zeitoun-Fakiris, A. and Juttner, B. (1991) On the dose of bombarding residual gas ions for influencing pre-breakdown field emission in vacuum. *J. Phys. D*, **24**, 750.

56. Chalamala, B.R., Reuss, R.H., and Dean, K.A. (2001) *Appl. Phys. Lett.*, **78**, 2375.

57. Yotani, J., Uemura, S., Nagasako, T., Kurachi, H., Yamada, H., Ezaki, T., Maesoba, T., Nakao, T., Saito, Y., and Yumura, M. (2003) *Soc. Inf. Disp. Digest*, **34**, 918.

58. Dean, K.A. and Chalamala, B.R. (1999) *Appl. Phys. Lett.*, **75**, 3017.

59. Holland, L. and Ojha, S.M. (1976) The chemical sputtering of graphite in an oxygen plasma. *Vacuum*, **26**, 233.